USGS
science for a changing world

Prepared for the National Aeronautics and Space Administration

Geologic Map of the Artemis Chasma Quadrangle (V–48), Venus

By Roger A. Bannister and Vicki L. Hansen

Pamphlet to accompany
Scientific Investigations Map 3099

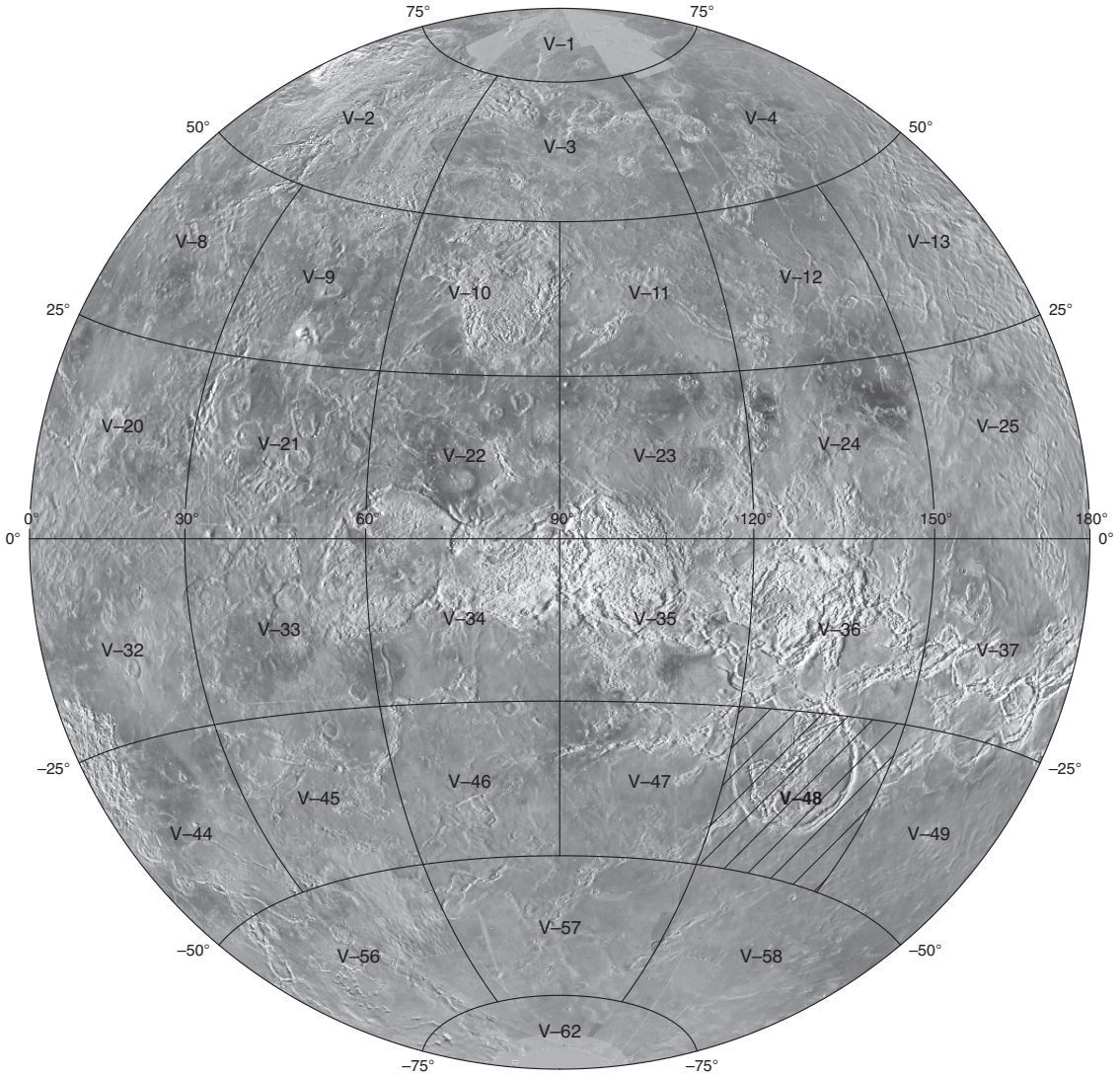

2010

U.S. Department of the Interior
U.S. Geological Survey

Contents

Figures

Tables

The Magellan Mission

The Magellan spacecraft orbited Venus from August 10, 1990, until it plunged into the Venusian atmosphere on October 12, 1994. Magellan Mission objectives included (1) improving the knowledge of the geological processes, surface properties, and geologic history of Venus by analysis of surface radar characteristics, topography, and morphology and (2) improving the knowledge of the geophysics of Venus by analysis of Venusian gravity.

The Magellan spacecraft carried a 12.6-cm radar system to map the surface of Venus. The transmitter and receiver systems were used to collect three data sets: (1) synthetic aperture radar (SAR) images of the surface, (2) passive microwave thermal emission observations, and (3) measurements of the backscattered power at small angles of incidence, which were processed to yield altimetric data. Radar imaging and altimetric and radiometric mapping of the Venusian surface were accomplished in mission cycles 1, 2, and 3 from September 1990 until September 1992. Ninety-eight percent of the surface was mapped with radar resolution on the order of 120 m. The SAR observations were projected to a 75-m nominal horizontal resolution, and these full-resolution data compose the image base used in geologic mapping. The primary polarization mode was horizontal-transmit, horizontal-receive (HH), but additional data for selected areas were collected for the vertical polarization sense. Incidence angles varied between about 20° and 45°.

High-resolution Doppler tracking of the spacecraft took place from September 1992 through October 1994 (mission cycles 4, 5, 6). Approximately 950 orbits of high-resolution gravity observations were obtained between September 1992 and May 1993 while Magellan was in an elliptical orbit with a periapsis near 175 km and an apoapsis near 8,000 km. An additional 1,500 orbits were obtained following orbit-circularization in mid-1993. These data exist as a 75° by 75° harmonic field.

Magellan Radar Data

Radar backscatter power is determined by (1) the morphology of the surface at a broad range of scales and (2) the intrinsic reflectivity, or dielectric constant, of the material. Topography at scales of several meters and larger can produce quasi-specular echoes, and the strength of the return is greatest when the local surface is perpendicular to the incident beam. This type of scattering is most important at very small angles of incidence, because natural surfaces generally have few large tilted facets at high angles. The exception is in areas of steep slopes, such as ridges or rift zones, where favorably tilted terrain can produce very bright signatures in the radar image. For most other areas, diffuse echoes from roughness at scales comparable to the radar wavelength are responsible for variations in the SAR return. In either case, the echo strength is also modulated by the reflectivity of the surface material. The density of the upper few wavelengths of the surface can have a significant effect. Low-density layers, such as crater ejecta or volcanic ash, can absorb the incident energy and produce a lower observed echo. On Venus, a rapid increase in reflectivity exists at a certain critical elevation above which high-dielectric minerals or coatings are thought to be present. This leads to very bright SAR echoes from virtually all areas above that critical elevation.

The measurements of passive thermal emission from Venus, though of much lower spatial resolution than the SAR data, are more sensitive to changes in the dielectric constant of the surface than to roughness. They can be used to augment studies of the surface and to discriminate between roughness and reflectivity effects. Observations of the near-nadir backscatter power, collected using a separate smaller antenna on the spacecraft, were modeled using the Hagfors expression for echoes from gently undulating surfaces to yield estimates of planetary radius, Fresnel reflectivity, and root-mean-square (rms) slope. The topographic data produced by this technique have horizontal footprint sizes of about 10 km near periapsis and a vertical resolution on the order of 100 m. The Fresnel reflectivity data provide a comparison to the emissivity maps, and the rms slope parameter is an indicator of the surface tilts, which contribute to the quasi-specular scattering component.

Introduction

Artemis, named for the Greek goddess of the hunt, represents an approximately 2,600 km diameter circular feature on Venus, and it may represent the largest circular structure in our solar system. Artemis, which lies between the rugged highlands of Aphrodite Terra to the north and relatively smooth lowlands to the south, includes an interior topographic high surrounded by the 2,100-km-diameter, 25- to 200-km-wide, 1- to 2-km-deep circular trough, called Artemis Chasma, and an outer rise that grades outward into the surrounding lowland (fig. 1, on map sheet). Although several other chasmata exist in the area and globally, other chasmata have generally linear trends that lack the distinctive circular pattern of Artemis Chasma. The enigmatic nature of Artemis has perplexed researchers since Artemis Chasma was first identified in Pioneer Venus data. Although Venus' surface abounds with circular to quasi-circular features at a variety of scales, including from smallest to largest diameter features: small shield edifices (>1 km), large volcanic edifices (100–1,000 km), impact craters (1–270 km), coronae (60–1,010 km), volcanic rises and crustal plateaus (~1,500–2,500 km), Artemis defies classification into any of these groups. Artemis dwarfs Venus' largest impact crater, Mead (~280 km diameter); Artemis also lacks the basin topography, multiple ring structures, and central peak expected for large impact basins. Topographically, Artemis resembles some Venusian coronae; however Artemis is an order of magnitude larger than the average corona (200 km) and about twice the size of Heng-O Corona (which is 1,010 km in diameter), the largest of Venusian coronae. In map view Artemis' size and shape resemble volcanic rises and crustal plateaus; however, both of these classes of features differ topographically from Artemis. Volcanic rises and crustal plateaus form broad domical regions, and steep-sided regions with flat tops, respectively; furthermore, neither rises nor plateaus include circular troughs. So although it seems clear what Artemis is not, there is little

consensus about what Artemis is, much less how Artemis formed.

Debate during the past decade has resulted in the proposal of at least four hypotheses for Artemis' formation. The first (herein referred to as H1) is that Artemis Chasma represents a zone of northwest-directed convergence and subduction (McKenzie and others, 1992; Brown and Grimm, 1995; Schubert and Sandwell, 1995; Brown and Grimm, 1996). The second hypothesis (herein referred to as H2) is that Artemis consists of a composite structure with a part of its interior region marking the exposure of deformed ductile deep-crustal rocks analogous to a terrestrial metamorphic core complex (Spencer, 2001). The third (herein referred to as H3) is that Artemis reflects the surface expression of an ancient (>3.5 Ga) huge bolide impact event on cold strong lithosphere (Hamilton, 2005). The fourth hypothesis (herein referred to as H4) is that Artemis marks the surface expression of a deep mantle plume (Griffiths and Campbell, 1991; Smrekar and Stofan, 1997; Hansen, 2002; Ivanov and Head, 2003). Each of these hypotheses holds different implications for Venus geodynamics and evolution processes, and for terrestrial planet processes in general. Viability of H1 would provide support that terrestrial-like plate-tectonic processes once occurred on Earth's sister planet. The feasibility of H2 would require high values of crustal extension and therefore imply that significant horizontal displacements occurred on Venus—displacement that may or may not be related to terrestrial-like plate-tectonic processes. The possibility of H3 would suggest that Venus' surface is extremely old, and that Venus has experienced very little dynamic activity for the last 3.5 billion years or more; this would further imply that Venus is essentially tectonically dead, and has been for most of its history. This view contrasts strongly with studies that highlight a rich history of Venus including activity at least as young as 750 million years ago, and quite likely up to the present (for example, contributions in Bouger and others, 1997). If H4 has credibility, then Artemis could provide clues to cooling mechanisms of Earth's sister planet. Each of these hypotheses might be tested through geologic mapping aimed at unraveling the geologic history of Artemis and its surroundings. Artemis lies almost completely within the bounds of the Artemis Chasma quadrangle, V–48, which encompasses more than seven million square kilometers of Venus' southern hemisphere, extending from 25° to 50° S. and 120° to 150° E. Thus, construction of a 1:5 million-scale geologic map of Artemis Chasma quadrangle allows for unraveling the geologic history of Artemis to test various hypotheses of Artemis' evolution.

As a result of geological mapping, we propose a hybrid hypothesis for Artemis' formation. The hybrid hypothesis, which represents a modification to the plume hypothesis, involves the formation of an interior spreading center and newly formed crust, similar to that formed at a terrestrial divergent planet-boundary, as a result of a mantle plume; shortening of this crust within the chasma, which moves outward with continued formation of interior crust, might represent a failed Venusian attempt at subduction; the surface crust did not recycle to the mantle. Interior tectonomagmatic centers form broadly synchronously with interior crust formation. It is unclear when Artemis formed within Venus' evolution, although we postulate that it formed on thin lithosphere. Through this hybrid hypothesis we postulate that Artemis may record Venus' failed attempt at terrestrial plate-tectonic-like processes.

Venus

Venus, commonly referred to as Earth's sister planet, nearly equals the Earth in size, bulk density, and distance from the Sun; these similarities suggest that the bulk composition and heat budget of Venus should be broadly similar to the Earth (see Grimm and Hess, 1997). Despite these similarities, Earth and Venus evolved quite differently. Conditions at the Venusian surface are inhospitable to humans and life as we know it—with a temperature of approximately 760 K (~480° C), a caustic, dominantly CO2 atmosphere at a pressure of approximately 92 bars, and only trace amounts of water. The Earth's crust differentiated into granitic continental crust and basaltic oceanic crust, which is reflected in the bimodal distribution of the hypsometric curve for the Earth. Limited geochemical evidence from a series of Soviet Venera lander missions indicates that the Venusian surface likely resembles basalt (Barsukov and others, 1982; Surkov and others, 1986). The hypsometric curve for Venus displays a unimodal distribution implying that Venus' crust is not differentiated in the same manner as the Earth (Rosenblatt and others, 1994). Terrestrial plate-tectonic processes—manifested in long curvilinear features such as orogenic belts, subduction zones, oceanic spreading centers, and transform fault zones—provide a mechanism for interior heat to escape to the surface on Earth. Venus lacks such globally pervasive curvilinear features; instead, circular features dominate its surface, and their presence suggests that Venus loses its heat in a different manner (for example, Solomon and others, 1991; Solomon, 1993; Phillips and Hansen, 1994, 1998; Nimmo and McKenzie, 1998).

Terminology: Artemis Chasma, Artemis Corona, and Artemis

Artemis Chasma was first identified in low-resolution radar data from the NASA Pioneer Venus Orbiter mission. Stofan and others (1992) categorized Artemis Chasma, the interior region, and outer high as a corona after Magellan SAR data became available; however, due to considerations of size and possible different mechanism of formation, Artemis is no longer considered a corona (Stofan and others, 2001). Regardless, Artemis is referred to as "Artemis Corona" in some literature. The term corona (from the Latin word meaning "crown,") originated as a descriptive term for any quasi-circular structure defined primarily by an annulus of concentric fractures and/or ridges. The term gained genetic connotations as the body of corona research grew. Most researchers favor diapiric mechanisms for the formation of coronae (Squyres and others, 1992; Stofan and others, 1992; Koch and Manga, 1996; Smrekar and Stofan, 1997; Stofan and others, 1997; Hansen, 2003). However, the diversity of morphologies and range of sizes indicate that coronae may form by non-diapiric processes as well, including caldera collapse (Squyres and others, 1992; Roberts and Head, 1993;

DeLaughter and Jurdy, 1999) and/or bolide impact (for example, Barsukov and others, 1984, 1986; Basilevsky and others, 1987; Campbell and Burns, 1979; Grieve and Head, 1981; Head and Solomon, 1981; Masursky and others 1980; Schaber and Boyce, 1977; Nikolayeva and others, 1986; Greeley, 1987; Nikolayeva , 1993; Schultz, 1993; Hamilton, 2005; McDaniel, 2005; McDaniel and Hansen, 2005; Vita-Finzi and others, 2005). Although Stofan and others (1992; 1997) suggested that the wide range in corona morphology represents different stages of corona development, coronae display no obvious age progression where they occur in chains or clusters (see Hamilton and Stofan, 1996; Stofan and others, 1997; Hansen and DeShon, 2002). The vast size differences between Artemis and mean corona diameter (200 km), and between Artemis and Heng-O, raise concern over classifying Artemis as a corona. In this contribution we use the term 'Artemis' to refer to the entire large circular geomorphic feature centered at 33° S., 133° E., including Artemis Chasma, the raised interior region, and the adjacent exterior region (fig. 1, on map sheet), following terminology of Hansen (2002). This broad definition of Artemis helps to distance discussion from possible genetic connotations and/or assumptions associated with the term corona.

Data and Methods

The NASA *Magellan* mission (1991 – 1994) produced an amazing correlated digital geophysical data set for Venus with nearly global (approximately 98 percent) coverage (Saunders and others, 1992; Ford and others, 1993). The *Magellan* radar sensor acquired data in three modes: synthetic aperture radar (SAR), radiometer, and altimeter mode. The system used a 3.7-m diameter parabolic high-gain antenna (HGA) fixed 25° off nadir perpendicular to the trajectory of the spacecraft in SAR and radiometer modes. The SAR operated with a 12.6-cm wavelength at 2.385 GHz (S-band) with horizontal parallel transmit/receive polarization (HH) in order to penetrate the thick, CO_2-dominated cloud cover. SAR images were produced in three cycles with varying look geometries, and covering approximately 98 percent of the planet surface. Owing to the elliptical orbit, the SAR incidence angle was varied with latitude to provide an optimum signal-to-noise ratio. In the Artemis region incidence angles range from approximately 38–23°, approximately 25°, and approximately 20–14° from north to south for cycles 1, 2, and 3, respectively. SAR resolution is approximately 100 m/pixel. The altimeter mode used a smaller altimeter horn antenna (ALTA) fixed in the nadir direction. The size of the altimeter footprint varies with spacecraft altitude and therefore varies with latitude. In the Artemis region footprints measure 8–11 km in along-track dimension and 19–24 km in cross track dimension (Ford and others, 1993). Combining the surface-to-spacecraft distance with the known position of the spacecraft relative to the planetary center produces a global topographic data record (GTDR) with horizontal resolution approximately 10 km and vertical resolution approximately 80 m. Reflectivity and RMS-slope data sets were also derived from the altimetry data. Emissivity data were derived from radiometry measurements interleaved with the SAR observations. Gravity data were collected during cycles 4 and 5 before the spacecraft was intentionally crashed into the surface as a result of an effort to circularize the polar orbit to increase gravity data resolution in the polar regions of Venus.

Data for this study were provided by the USGS Astrogeology Team in the projection parameters for the Artemis Chasma (V–48) quadrangle (Lambert conformal conic, standard parallels at 34° S. and 73° S., central meridian 135° E., latitude of origin 90° S.). Left-look (cycle 1) F-MIDR (approximately 75 m/pixel), left-, right-, and stereo-look (cycles 1–3) C1-MIDR (approximately 225 m/pixel) SAR imagery were used in TIFF format, as were elevation, emissivity, RMS-slope and reflectivity data. The data used in this study are available online from the USGS Map-a-planet website (http://pdsmaps.wr.usgs.gov/) and the USGS Planetary GIS Web Server (PIGWAD, http://webgis.wr.usgs.gov/) in a variety of formats, although not necessarily in the projection parameters used herein. This study primarily uses SAR image mosaics from cycles 1, 2, and 3, including both left-looking and right-looking images. Cycle 1 left-looking SAR and cycle 2 right-looking SAR coverage of Artemis is nearly complete, whereas cycle 3 stereo data is extremely patchy. Compressed once (C1-MIDR) and compressed twice (C2-MIDR) SAR images are used for regional analysis, whereas full resolution images (F-MIDR) are used for detailed analysis of areas of interest (resolution of SAR images are 225, 675, and 75 m/pixel, respectively). GTDR data is used for analysis of regional topography and to assist in visualization in three dimensions.

Stereo imagery can greatly enhance the interpretation of landforms by displaying data in three dimensions. This technique works because parallax differences between two images with different viewing geometries produce a sense of depth when viewing the images with a stereoscope (or with red-blue glasses if the images are combined to form a red-blue anaglyph). In the case of *Magellan* SAR data, image pairs with opposite look directions are difficult to visually merge because the illumination direction changes drastically between the two images; however, stereo pairs with the same look direction but different incidence angles (for example, cycle 1 and cycle 3 left-look SAR images) can be combined to great effect (Plaut, 1993). Although true stereo coverage of Artemis is poor due to the paucity of cycle 3 data, we used synthetic stereo images (Kirk and others, 1992) constructed with C1 SAR images and altimetry data using a custom program and macros authored by Duncan A. Young. Although regional topographic trends are easily gleaned from synthetic stereo images, this data set does not resolve subtle topographic features that might be resolved in true stereo images.

Radar Interpretation

Radar image brightness is a function of the roughness, topography, and electrical properties of the imaged surface. Surfaces that are inclined towards the incident radar and/or are rough at or above the scale of the radar wavelength (12.6 cm) appear radar-bright; surfaces that are inclined away from

the incident radar and/or are smooth (below the scale of the radar wavelength) appear radar-dark (Ford and others, 1993). The opposite is true for inverted SAR images. Inverted SAR images are useful for structural analysis because structural elements (typically lineaments) tend to be more visible than in normal SAR images (Hansen, 2000). Due to the geometry of radar, echoes from areas of high elevation return to the antenna before echoes from areas of low elevation. This causes mountain peaks to image forward of their actual position, known as foreshortening; the opposite occurs on the back slope, known as elongation. If the echo from the peak returns before the echo from the forward toe, then the peak will be imaged on top of the base, an effect known as lay-over. A surface inclined away from the radar look direction at an angle greater than the incidence angle will lie in radar shadow and will not be imaged. These effects complicate SAR image interpretation but once understood, SAR images can provide a tool for determining short-wavelength topography. For a more complete discussion of the interpretation of Magellan SAR data, see Ford and others (1993).

Mapping Methodology

Geologic mapping was conducted according to guidelines set forth by Wilhelms (1990) and Tanaka and others (1994) with caveats highlighted by Hansen (2000), Zimbelman (2001), and Tanaka and others (2010). Within the Artemis quadrangle we differentiate primary and secondary structures, structural domains, terrain units, material units, and radar facies. Primary and secondary structures are commonly defined based on morphology and regional patterns. By definition, primary structures formed during material unit emplacement whereas secondary (tectonic) structures record post-emplacement deformation. Structural domains comprise regions marked by closely spaced tectonic fabrics, and they typically show spatial correlation with regional morphologic features. Terrain units are defined texturally by penetratively developed secondary structures, and they indicate a shared geologic history of materials after the emplacement/formation of secondary structures that combined potentially previously unrelated material units. Terrain units do not imply a shared history or genetic relationship prior to the deformation event(s) responsible for the imparting of their characteristic (structural/tectonic) textures. Material units are defined by morphology, primary structures, and radar characteristics; material units are interpreted as representing coherent units emplaced in discrete periods of geologic time. Radar facies units represent surface areas that we were not comfortable uniquely interpreting as either a terrain unit or a material unit, that is, the character of radar facies units reflect radar properties that *might not b*e uniquely attributed to material properties or tectonic properties; in fact, the radar signature could reflect a combination of material and tectonic characteristics at the effective resolution of the current data. The character and distribution of primary structures, secondary (tectonic) structures, structural domains, terrain units, and material units all provide clues to surface material properties (for example, rheology), geologic history, and formative processes.

Background

Artemis lies almost completely within the V–48 quadrangle (fig. 1 and map sheet). The V–48 map area is bounded to the north by the rugged Aphrodite Terra highland, but it is separated from this highland region by Quilla Chasma. To the northeast, the east-northeast-trending corona-chasmata chain of Diana-Dali feathers out just outside the V–48 quadrangle. A second, northeast-trending corona chain, south of the Diana-Dali chain, barely kisses the east margin of the map area, and it ends with Teteoinnan Corona in V–48. Annapurna and Colijnsplaat Coronae, also part of this chain, lie mostly within the V–49 quadrangle to the east. To the southeast, south, and southwest of Artemis, Zhibek, Laimdota, and Anio Planitiae, respectively, mark vast expanses of lowland. East-trending Juno Chasma occurs to the west of Artemis and the V–48 map area. Artemis dominates V–48, and understanding its formation represents the focus of this study.

Previous Work

Geologic Mapping

At least three independent groups have published regional scale geologic maps covering at least part of Artemis. Brown and Grimm (1995), who focused mapping efforts on Artemis Chasma, published a simplified tectonic sketch map. They used *Magellan* data, as we do, although their visualization techniques differ from ours. These workers used the "magic-airbrush" technique (Kirk and others, 1992) to create shaded-relief images; this technique operates on the premise that the surface roughness and dielectric constant contributions to radar signal strength should be similar between left- and right-look images, whereas the slope effects should be quite different. By calculating a weighted difference between left- and right-look images, which effectively removes the roughness and dielectric constant components, only the slope component of image brightness remains. Although this method produces shaded-relief images at the resolution of the SAR imagery, it preserves radar foreshortening and elongation effects, particularly in regions of high topographic relief or steep slopes, such as parts of Artemis' interior and along/within Artemis Chasma. Hansen (2002) published a reconnaissance geologic map that includes a broad look at Artemis' interior, chasma, and exterior regions; this work is less detailed than the current mapping effort. Hansen (2002) used *Magellan* SAR images and topography data; inverted SAR images were used to highlight structural lineaments, and synthetic stereo images that combined SAR and topographic relations allowed three-dimensional visualization (Kirk and others, 1992). The geologic maps of Brown and Grimm (1995) and Hansen (2002) broadly agree in the location and characterization of structural features, although the interpretations of these workers follow quite different paths. Hansen's (2002) map covers a slightly larger region and is more detailed both in structural notation and in the consideration of geologic units, as expected for a later work. Spencer (2001) produced a sketch map of the "central interior deformation belt," through the examination of secondary structures within a

limited region within Artemis' interior. The sketch map shows a relatively low level of detail, and although it was published after the efforts of Brown and Grimm (1995), the sketch map is not presented in the context of that earlier work.

Gravity Analysis

Schubert and others (1994) analyzed *Magellan* gravity data of large coronae and numerous chasmata. A semi-circular positive gravity anomaly of 20–40 mgal lies along Artemis Chasma, most prominently expressed in the southeast part of the interior. Schubert and others (1994) calculated a best-fit apparent depth of compensation (ADC) of 200±12.5 km for the large gravity anomaly and about 50±12.5 km for the Artemis region in general, a gravity/topography ratio of 0.056±0.008 mgal/m, and a geoid/topography ratio of 35±5 m/km for the Artemis region. Gravity analyses provide some insight into subsurface structure; however, interpretations of lithosphere structure based on gravity are inherently non-unique and dependent on analysis and embedded assumptions. For instance, the gravity/topography data for Artemis is consistent with partial dynamic support, thick lithosphere (>100 km), or a combination thereof (Schubert and others, 1994; Simons and others, 1997).

Modeling

Artemis has been the focus of, or referred to within, flexural modeling, fluid-dynamics experiments, and finite-element modeling. Inelastic and elastic flexural modeling (Brown and Grimm, 1996), which hinges on the proposal that Artemis Chasma is analogous to terrestrial subduction zones (for example, Sandwell and Schubert, 1992; Brown and Grimm, 1995; Schubert and Sandwell, 1995), aims at estimating local geothermal gradient and lithospheric rheology. Brown and Grimm (1996) focused modeling on the southeast part of Artemis Chasma because that is where the chasma trends perpendicular to proposed northwest-directed convergence; the northeast- and southwest-trending parts of Artemis Chasma were not addressed through modeling. Fluid-dynamics laboratory experiments aimed at modeling the interaction of terrestrial plume-lithosphere interactions (Griffiths and Campbell, 1991), serendipitously found application to Artemis. Griffiths and Campbell (1991) noted that as a plume head approaches a rigid boundary it flattens and spreads laterally; 'mantle' material squeezes out from between the plume head and the rigid layer (lithosphere), and a ring-shaped instability develops to form an axisymmetric trough. Noting the similarity of the experimentally formed trough with Artemis Chasma, which had only recently been imaged by *Magellan* SAR data, Griffiths and Campbell (1991) proposed that Artemis might represent the surface expression of a large thermal mantle plume (the term 'plume' infers thermal, as opposed to compositional buoyancy [Griffiths, 1986a, b]). Finite-element modeling of the interaction of a large thermal mantle plume with the lithosphere, aimed at modeling Venusian corona topography (Smrekar and Stofan, 1997), also resulted in the formation of an axisymmetric trough, and it may provide further support for a plume origin for Artemis.

Geology of Artemis Chasma Quadrangle

Geologic Relations

V–48 includes Artemis, the termination of a northeast-trending corona chain marked by Teteoinnan Corona, the northwestern part of Zhibek Planitia, the northern extent of Laimdota Planitia, and a tiny part of the easternmost part of Aino Planitia (fig. 2 and map sheet). A northeast-trending fracture zone trends toward Artemis from the southwest. East-trending Juno Chasma lies completely to the west of V–48, outside the quadrangle. Lava flows sourced from Inari Corona and Quilla Chasma to the north spill into the northwest corner of V–48 and Artemis' interior. Lava flows from Ceres, Bona and Miralaidji Coronae spill into the northeast corner of V–48. As noted, this study focuses on the formation of Artemis.

Artemis is composed of an interior region, Artemis Chasma, and an outer high. The interior of Artemis hosts four spatially and temporally overlapping tectonomagmatic centers (*TMa–d).* Britomartis Chasma trends northeast through the northernmost tectonomagmatic center (*TMd*). A regionally extensive, penetratively developed, tectonic fabric characterizes much of Artemis' interior. This interior penetrative fabric, marked by tightly spaced lineaments (average wavelength 500 m), generally trends northeast, although it locally changes trend near the tectonomagmatic centers. Artemis Chasma hosts a trough-parallel lineament fabric marked by closely spaced lineaments; the tectonic chasma fabric differs from the interior penetrative tectonic fabric in trend and spacing, being generally more widely spaced. Outside and exterior to the chasma an extensively developed suite of wrinkle ridges broadly parallels the concentric trace of the chasma. A 300-km-wide fracture zone trends northeast toward the chasma along the southwestern margin, and a chain of coronae developed to the east of Artemis, mostly outside the V–48 quadrangle. Locally, flows sourced from Artemis' interior extend across the western part of the chasma, and they are locally buttressed by topographic expression of the chasma tectonic fabric along the south and east margins; these relations indicate that evolution of the interior region and the chasma temporally overlapped, at least in part. Temporal relations between the chasma and the fracture zone are unclear, although our results suggest broadly synchronous evolution of the chasma trough and the fracture zone.

We present geologic relations by region, starting with the exterior and working inward. Prior to this discussion we introduce primary and secondary structures and impact features that occur across and within the V–48 map area; primary structures and impact features are also discussed in the context of geologic descriptions of the individual regions: exterior, chasma, and interior. In our discussion of geologic history, we reverse the order and discuss evolution from the interior outward.

Primary and Secondary Structures

Primary and secondary structures defined within the Artemis quadrangle are described herein; individual map units and structural domains are described within the regional context

in which they are found. For discussion purposes we divide Artemis morphologically into the chasma, exterior, and interior regions. Artemis Chasma, defined topographically by radial clock position, extends from approximately 12:00 clockwise to 10:30, with its deepest and steepest topographic expression occurring from approximately 2:00 clockwise to 7:00. Secondary structures generally parallel the concentric trend of the chasma, although locally structures trend normal to chasma-tangent trends. The exterior includes (a) chasma-concentric wrinkle ridges, (b) chasma-normal radial fractures, (c) a northeast-trending fracture zone also marked by a northeast-trending topographic trough that occurs to the southwest of Artemis, and (d) a chain of coronae developed to the east of Artemis. Within its interior Artemis preserves four tectonomagmatic centers; interior map units roughly divide into two groups. These groups are radar-rough tectonic terrains (units tAa and tAb) and radar-smooth volcanic flow materials (units fcAa, fcAb, fsAa, fsAb, fsAc, fu, and flu). A penetrative tectonic fabric developed in units tAa and tAb occurs across much of the interior. Radial and concentric structural suites and associated flows define four centers of tectonic and magmatic activity (*TMa–d*). The three divisions of Artemis—chasma, exterior, and interior—host division-specific map units, and, commonly, tectonic structural patterns. Only two units, unit fu (undivided flows) and unit fcAa (a flow unit), occur across these divisions. Unit rf (radar facies) occurs within the exterior and crosses into the chasma locally. One suite of structures, shallow troughs, extends from the interior across the chasma to the exterior along Artemis' western margin. Other suites of primary or secondary structures are generally spatially limited to defining patterns within one of the three regions, although exterior radial fractures extend slightly into the outer reaches of the chasma.

By definition primary structures form during the emplacement of geologic units, and their character may assist in defining the spatial limits of individual material units. SAR images of primary structures within V–48 are shown in figure 3 and include shields, channels, pit chains, flow fronts, shallow troughs, and crater rim crests. *Shields* are small (<1–15 km in diameter) circular to quasi-circular features with dome, cone, shield, or flat-topped shapes that may or may not contain a central pit (Guest and others, 1992; Crumpler and others, 1997; Addington, 2001), interpreted as small volcanic edifices. *Channels* are narrow (generally about 1 km) steep-sided, shallow (on the order of tens of meters), sinuous troughs morphologically similar to terrestrial fluvial channels, interpreted to form by channelized fluid flow (Baker and others, 1992; Komatsu and Baker, 1994; Baker and others, 1997). The nature of the fluid is undefined, as is the type of erosion, whether mechanical or thermal, cutting downward from the surface, or upward from depth (for example, Gregg and Greeley, 1993; Bussey and others, 1995; Williams-Jones and others, 1998; Jones and Pickering, 2003; Lang and Hansen, 2006). *Pit chains* are a collection of small (<1–10 km diameter) sharply defined circular to elliptical depressions arranged in a line, interpreted as the result of stoping of material marking the surface expression of dilatational dikes or faults (Okubo and Martel, 1998; Ferrill and others, 2004). Pit chains can be considered either primary or secondary structures depending on the question at hand. *Flow fronts* are lobate margins of discrete lava flows (Chapman, 1999). *Shallow troughs* are a pair of closely spaced (<5 km) lineaments marking a shallow (tens of meters) flat depression bounded by steep sides; they are interpreted herein as the result of subsurface magmatic activity. *Crater rim crest is* the raised rim of an impact crater enclosing an interior basin. *Flow direction*, although not a primary structure but interpreted from primary structures (for example, channels, levees, and other flow constructs), is also shown. In addition we indicate local *radar boundaries*, marked by a sharp transition in radar brightness; these boundaries commonly show lobate character, although we are not confident that they represent flow fronts or necessarily primary structures. In fact, different radar boundaries might represent different features or have a range of implications for surface geology as well as geologic history.

Secondary structures, by definition, form after the emplacement of geologic units and typically record tectonic processes; accordingly, they provide clues for operative tectonic processes. In addition, the distribution and (or) character of secondary structures may provide clues for the delineation of material units, as well as temporal relations between different material units (Hansen, 2000; Tanaka and others, in press). SAR images of secondary structures within V–48 are shown in figure 4 and include fractures, folds, small ridges, large ridges, interior penetrative fabric, and lineaments. *Fractures* are extremely sharp lineaments with a negative, or null, topographic signature, commonly grouped into suites based on orientation, pattern (namely, radial or concentric) and/or spacing (that is, widely spaced or closely spaced). Fractures are generally interpreted as extensional structures (Banerdt and others, 1997). *Folds* are ridges with a gradational radar character, normal to their trend, and wave-like topographic expression; they are generally interpreted as contractional structures (Stofan and others, 1993). *Small ridges* are topographic ridges with low relief and width, similar in appearance to folds except that the nature of the lineaments is ambiguous—though possibly of contractional origin (marked by folds or thrust faults). *Large ridges* are topographic ridges with moderate relief and width. *Interior penetrative fabric* represents closely spaced (0.5–1 km) lineaments with slight gradation in radar brightness across strike. It is interpreted in some cases as short-wavelength low-amplitude folds, and in other cases as fracture-like structures; however, in many cases the fabric character is ambiguous (also see fig. 5). *Lineament* is a discrete feature with possible ambiguous topographic expression and undetermined origin, yet interpreted as likely tectonic in origin.

Four structural fabric domains are delineated on the map: (1) fracture zone penetrative fabric, (2) chasma penetrative fabric, (3) interior penetrative fabric, and (4a) short, closely spaced wrinkle ridges occur within Artemis, and (4b) outside of Artemis northeast of the northeast-trending portion of Artemis Chasma. The three penetrative fabrics (1–3) comprise areally extensive tectonic (?) fabrics developed at the scale of current SAR effective resolution; the spatial extent of each fabric does not necessarily correspond with a material unit (see Hansen, 2000). Each fabric domain is discussed in the context of its regional location.

Impact Features

The V–48 quadrangle hosts seven to nine impact craters that range in diameter from 4.5 to over 87 km (table 1). Seven of these features are noted in the two Venus crater databases (Schaber and others, 1992; Herrick and others, 1997). Schaber and others (1992) interpreted Ivne, the eighth feature, as a double impact crater; however, Ivne is not included in Herrick and others' (1997) crater database. We favor the interpretation of Herrick and others (1997)—that is, Ivne is not an impact crater. In left-look SAR images, Ivne appears to be marked by two overlapping circular features (7 km and 9 km in diameter, which are stacked north to south). However, in right-look SAR images, only the southern feature is visible, and it is characterized by a diameter of about 4 km, as well as poor 'rim' definition along the north and south regions. No clear ejecta blanket or halo is visible in either SAR data set. The ninth feature is a possible impact crater, although this feature is not represented in either crater database.

Essentially all of the confirmed impact craters show ejecta blankets, and two show clear halo deposits. The lack of crater halos might reflect the small size of the craters, or it could record halo removal (see Izenberg and others, 1994). The four largest craters have radar-smooth interiors, interpreted as interior fill; the small craters do not show clear radar-smooth interiors, although this may be a function of their small size, rather than direct evidence of the character of their interiors. Crater-density values range from 0.96 to 2.55 craters/10^6 km^2 (Herrick and others, 1997). Crater density might reflect the relative age of a composite surface. Only one crater (O'Connor) has a crater density value that is higher than Venus' global average (approximately 2 craters/10^6 km^2; Phillips and Izenberg, 1995; McKinnon and others, 1997). The calculated crater density values do not, however, include Ivne or the newly identified feature, which could (but might not) be impact craters. In any case, Venus preserves far too few craters to robustly constrain the age of any individual surface, much less individual geologic unit, across the planet in general, or V–48 specifically (Hauck and others, 1998; Campbell, 1999).

Exterior Region

The exterior region of V–48 includes the topographically defined outer high. Clockwise from the east, this region encompasses a northeast-trending chain of coronae that just extends to the eastern boundary of V–48, the northwestern extent of Zhibek Planitia to the southeast, Biliku and Laverna Dorsa to the south, and a fracture zone that trends northeasterly toward the southwest margin of Artemis Chasma. The fracture zone lies along trend with northeast-trending Britomartis Chasma within Artemis' interior. The outer high forms a broad ridge that parallels the concentric form of Artemis Chasma. Radial fractures trend normal to Artemis Chasma from about 1:00 (the map area limit) clockwise to about 8:00. Wrinkle ridges, developed concentric to the chasma (and perpendicular to radial fractures), increase in spacing away from the chasma. The regional fracture suite trends normal to the trace of the outer high, and it forms an impressive radial pattern with foci in the center of Artemis' interior. The spacing and intensity of fractures varies across the exterior region with the most closely spaced fractures developed within the northeast-trending fracture zone. The fracture zone, as well as fractures within it, trends consistent with the radial pattern marked by the regional fractures. Wrinkle ridges also form an impressive concentric pattern across the exterior region. Like the regional fractures, the concentric center for the wrinkle-ridge pattern falls within the center of Artemis' interior region. Artemis Chasma, regional radial fractures, and wrinkle ridges all share the same center point (Hansen, 2002). Wrinkle-ridge spacing and intensity also vary across the exterior region; short, closely spaced wrinkle ridges parallel the chasma along the southern, southwestern, and western margins (though they do not occur along the region of intense fractures within the fracture zone); wrinkle ridges are both longer and more broadly spaced to the southeast and east. Along the western margin of the chasma, wrinkle ridges within the chasma and the exterior define the same trend, and they define a gradation in spacing. Along the northeastern margin of the chasma, at the northern boundary of the quadrangle, wrinkle ridges are also short and closely spaced. Short and closely spaced wrinkle ridges are present adjacent to the outer limit of the chasma, whereas longer and more widely spaced wrinkle ridges occur farther from the chasma. Along the outer high, outboard from the southeastern margin of the chasma, regional fractures describe a chasma-radial pattern, but wrinkle ridges are absent.

The corona chain east of Artemis trends northeast across V–49, Mahuea Tholus quadrangle. Teteoinnan Corona (38.5° S., 149.5° E.; 125 km in diameter), which marks the end of the corona chain, lies almost completely within V–48; Annapurna (35.5° S., 152° E.; 300 km diameter) and Colijnsplaat (32° S., 151° E.; 350 km in diameter) Coronae lie mostly within V–49, although associated fractures (and possibly flows in the case of Colijnsplaat) extend into V–48. Radial fractures define each of these three coronae; Colijnsplaat Corona also displays concentric fractures and possible flows. The corona chain defines the northwestern boundary of Zhibek Planitia, which occupies the southeastern part of V–48. Zhibek Planitia is relatively featureless here—it is marked by east-northeast-trending wrinkle ridges of the Artemis Chasma concentric suite and northwest-trending regional fractures that are radial to Artemis Chasma.

Biliku Dorsa (600 km long, 100 km wide) lies completely within Zhibek Planitia, whereas Laverna Dorsa (1,000 km long, 100 km wide) appears to form the boundary with Zhibek Planitia to the east and Laimdota Planitia to the west, although both planitiae lie mostly within V–58 and V–57, respectively, to the south of V–48. Biliku and Laverna Dorsa represent subtle topographic ridges that trend northwest and northeast, respectively. Laverna Dorsa extends into V–57 where the dorsa trend reverts to a northeast-trend, as marked by Sunna Dorsa (500 km long, 100 km wide) that broadly parallels Biliku Dorsa in V–48. The region west of Laverna Dorsa appears to be Laimdota Planitia, although Laimdota and Zhibek Planitiae are not clearly differentiated within V–48. The radial regional fractures and concentric regional wrinkle ridges occur across both Laimdota and Zhibek Planitiae. The northeast-trending fracture zone and the relatively radar-smooth region just northwest of the fracture

zone lie within either Laimdota Planitia or within Aino Planitia, which lies dominantly within V–47 to the west of V–48.

Three units, fcCBM (Ceres, Bona, and Miralaidji Coronae flow material, undivided), fu (flows, undivided) and rf (radar facies), dominate the exterior region. Unit fcCBM spills into V–48 in the northeast corner of the map area from its source region in V–37 to the northeast. This unit is correlative with unit fcCBM described by Hansen and DeShon (2002). Unit fu includes, as suggested by its name, a range of undivided, generally low radar-backscatter flows. In several locations (for example, 143° E., 40° S.) sharply defined radar boundaries occur. Elsewhere radar boundaries are more diffuse and gradational (for example, 140° E., 45° S.), but radar character definitely changes within and across unit fu. We do not interpret the various radar boundaries as necessarily marking distinct flow units given that distinct radar domains can occur within single geologic units (Tanaka and others, 2010). Given the current SAR resolution, the overall size of the map area, and the 1:5 million map scale, we cannot delineate individual material units with confidence, and thus unit fu, as shown within the study area, represents a composite unit that was almost certainly emplaced in a time-transgressive fashion and represents numerous varied material units. Unit rf includes the part of the radar-bright facies defined by Hansen (2002) associated with exterior coronae along the eastern margin of V–48. Hansen's (2002) radar-bright facies (volcanic and tectonic) is divided into several units in this mapping effort—these include unit rf discussed herein and a fracture zone fabric (both of which occur within the exterior region), chasma tectonic fabric (within Artemis Chasma), and the interior penetrative fabric and interior flow units, which occur within Artemis' interior. The chasma tectonic fabric and interior penetrative fabric together form 'fine-scale fabric' of Brown and Grimm (1995). Unit rf remains as a radar unit, as opposed to a geologic unit; it likely includes both tectonic fabrics and flows. The other 'units' are each interpreted herein as tectonic fabric facies, and they are discussed within the context of their areal domains. Unit rf shows high-radar backscatter, likely due to a combination of roughness due to fractures and surface layer roughness. Unit rf is spatially associated with Colijnsplaat Corona. Fracture terrain of Zhibek Planitia, unit frZ, marked by tightly spaced fractures, underlies unit fu, but it lies exposed in a local topographic high. It is not clearly understood whether unit frZ includes several distinct material units or a single unit; only the presence of tightly spaced fractures allow us to delineate this unit spatially and temporally from the overlying, and younger, composite unit fu. The limited spatial extent of unit frZ might favor a singular unit origin prior to fracture formation. Unit frZ lies along the southern extent of Laverna Dorsa, which shows a slightly higher density of dorsa-parallel fractures than the surrounding areas. Biliku Dorsa is similarly marked by slightly higher fracture density and by a slight z-shaped bend in otherwise north-northwest-trending fractures. Laverna Dorsa trends generally parallel to the regional fractures, whereas Biliku Dorsa trends at a high angle to the same fracture suite; both dorsa are quite subtle.

The approximately 300 km wide northeast-trending fracture zone that abuts the southwest part of Artemis Chasma along strike is defined as a structural domain marked by fracture zone fabric, rather than a terrain unit or material unit. As with the chasma tectonic fabric, a zonal pattern marks the spatial limit of the fracture zone fabric, whereas lines describe lineament trends. Fracture spacing diminishes outward normal to the trend of the fracture zone. The fracture zone appears to fade outward to the east, as marked by a gradual decrease in fracture spacing; however subsequent local or regional cover cannot be ruled out. The fracture zone is locally covered along its western reaches by shield terrain (unit s), which generally includes 1- to 4-km diameter edifices and associated flow material. Delicate interfingering of shield material into topographic lineaments indicates negative topographic expression of at least some of the fractures within the fracture zone. Unit s and unit fu are both time transgressive; as such, we cannot determine robust temporal relations between these units and therefore they are shown with essentially no temporal constraints.

Impact craters O'Connor and Jalgunik occur in the northeastern and southwestern parts, respectively, of the V–48 exterior region.

Artemis Chasma

Artemis Chasma forms a well-defined circular trough that encloses approximately three quarters of Artemis' interior. The chasma ranges in width from approximately 25 to approximately 200 km and displays an average relief of 1 to 2 km. Artemis Chasma fades away in the northwest (~10:30) and increases in width and depth to its maximum in the southeastern to eastern part of the chasma. The chasma appears to be defined topographically first, and second in terms of secondary structures; no material units define the chasma, and no units obviously embay the chasma. The chasma hosts a tectonic fabric that consists of trough-parallel lineaments with increasing intensity (decrease in spacing) clockwise to the southeast, and decreasing intensity (increase in spacing) to the northwest (Brown and Grimm, 1995; Hansen, 2002). The lineaments appear to form smooth ridges within the trough and along the inward facing (outside) chasma wall. We interpret these lineaments to be folds, in concurrence with Brown and Grimm (1995) and Hansen (2002). Brown and Grimm (1995) and Hansen (2002) also described chasma lineaments that occur along the interior chasma (outside facing) wall as normal faults; however, we cannot robustly determine the nature of these structures. We simply refer to these structures as lineaments; they could represent a combination of fractures, faults, and folds. Regardless of character, the spacing of the lineaments varies within the trough as noted, although the lineaments everywhere generally parallel the trend of the trough. We defined a structural domain, chasma penetrative fabric, wherein the lineaments become so closely spaced relative to the radar resolution that mapping individual lineaments at 1:5 million-scale is not viable; a stippled pattern shows the extent of the domain, whereas lines indicate lineament trend. At approximately 10:30, where the chasma narrows in width and shallows and fades topographically, chasma lineaments appear to become wrinkle ridges, parallel in trend to the trough, but with slightly wider spacing, and presumably lower height, than lineaments preserved counterclockwise within the

trough. There is no evidence that the trough or trough lineaments are buried by younger material; obvious embayment relations are lacking. For more detail about chasma structures see Brown and Grimm (1995) and Hansen (2002). The material that comprises the chasma, a homogeneous radar smooth unit (unit fu, flows undivided) appears contiguous with exterior material across much of the chasma, and it is contiguous with both the interior and exterior along the northwest region where the chasma lacks strong topographic definition. Although the chasma is marked by wrinkle ridges and folds with axes parallel to the concentric form of the chasmata, and by fractures that trend normal to the chasma, there is a slight deviation from this pattern at the exterior-chasma boundary at 6:00. Here the fractures mark a moderate radial pattern across approximately 170°; wrinkle ridges, orientated normal to the fractures, are shorter and more tightly spaced than wrinkle ridges away from the quasi-radial structure. Hansen (2002) referred to this structure as a corona (C6); we do not follow a corona interpretation herein because a (half) radial pattern of fractures does not, by itself, make a corona.

No impact craters are recognized within Artemis Chasma.

Interior Region

Artemis' interior makes up the bulk of the quadrangle and records the richest local geologic histories. The interior, which displays significantly more radar-rough facies as compared to the exterior region, includes four tectonomagmatic centers, defined by radial and/or concentric fractures or lineaments and discrete flows as well as the northeast-trending Britomartis Chasma, which extends from the near center of Artemis to the northeast chasma margin. Although Hansen (2002) described the tectonomagmatic centers as corona-like features, in the interest of objectivity we refer to them herein as tectonomagmatic centers, labeled *TMa–d* starting with the westernmost feature and proceeding in counterclockwise fashion. Britomartic Chasma appears roughly parallel to, and along trend with, the northeast-trending fracture zone within the exterior region, however feature *TMa* and Artemis Chasma separate the two zones. Additionally, the exterior fracture zone and Britomartic Chasma are each marked by quite different geomorphic features, as discussed below. Four major units occur within the interior region. Tectonic terrain units a and b of Artemis (units taA and tbA) occur across a northeast-trending outcrop that dominates the central region; composite flow material a and b of Artemis (units fcaA and fcbA) occur to either side of this, and it dominates the northwestern and southeastern interior regions, respectively. In addition, various flows and shield-related materials occur in association with individual tectonomagmatic centers, as described herein. Unit flu, localized flow material, undivided, occurs in small outcrops typically filling local topographic lows, particularly within Britomartic Chasma. Composite unit fu, which also occurs within Artemis Chasma and the exterior region, occurs within the northwestern part of the quadrangle and within the interior region. Unit fcl, flow material from Inari Corona, and unit fchQ, flow material of Quilla chasma, spill into V–48 from source areas to the north in V–35 and V–36, respectively. Unit fcl correlates with unit fl1b of Bleamaster and Hansen (2005). Each of the units within the northwestern corner of the quadrangle show gradational contacts with one another, except for unit fchQ, which has a well-defined unit boundary and appears to be the youngest of the units in this region. Artemis' interior also hosts a distinctive structural domain indicated on the map by a stipple pattern. Units taA and tbA each host a penetratively developed linear fabric, called 'interior penetrative fabric.' The fabric generally trends northeast across the interior with local deviation from this trend in spatial association with the tectonomagmatic centers. Locally, a fabric that consists of short, closely spaced wrinkle ridges occur within unit fcAb along the easternmost boundary of the interior and Artemis Chasma, and within unit fl1b in the northwest part of Artemis. Feature *TMa* (C4 and C3 of Hansen [2002]; southwestern interior deformation belt of Spencer [2001]) is defined by radial fractures, concentric ridges, weakly concentric fractures, radial flows, and the low-radar-backscatter material of unit fsAa (flows and shield-related material a of Artemis). A shallow topographic trough wraps from the northern margin counterclockwise to the southwestern margin of feature *TMa* (most of Brown and Grimm's [1995] north-northwest-trending deformation belt). Unit fsAa (flows and shield-related material a of Artemis) hosts numerous small shield edifices and surrounds kipukas of unit tAa (tectonic terrain of Artemis, unit a). Unit fsAa interfingers with unit tAa, and it fills long, narrow, shallow valleys within unit tAa. Unit fsAa locally covers earlier formed tectonic fabrics, but it is also cut by northeast-trending fractures that may represent reactivated buried structures. We interpret these relations to indicate that unit fsAa is locally thin (tens of meters) and had a low emplacement viscosity due to the intricate interactions with preexisting topography. Impact crater Bonnevie (approximately 80 km in diameter) lies along the eastern margin of unit fsAa. Robustly constraining temporal relations between Bonnevie and unit fsAa proves difficult due to the degraded state of the crater ejecta. The flow units may have been emplaced both prior to and after formation of Bonnevie. The crater interior is clearly flooded by radar-smooth material, taken here as flood lava. An interior central peak rises above the flooded crater interior. The eastern part of feature *TMa* (C3 of Hansen [2002]) hosts radial fractures that weakly define a secondary center. Flows emanate from the eastern margin and extend eastward and southeastward toward feature *TMb*. Veronica crater (17.9-km diameter) lies along the southern flank of feature *TMa*. Veronica appears to dominantly post-date the formation of the penetrative fabric, as indicated by radar-bright flows or impact ejecta that show spatial association with Veronica and appear to fill topographic lows within the penetrative fabric. Veronica might show fractures parallel to the penetrative fabric, although this observation is difficult to confirm. The interior of Veronica shows radar-smooth material not cut by fractures. Feature *TMb* (C2 of Hansen [2002]) is defined by: radial fractures, distal concentric fractures, and the low-backscatter material of unit fsAb. Unit fsAb hosts numerous small shield edifices with one approximately 5-km diameter volcanic edifice near the center. Unit fsAb surrounds kipukas of unit tAa and delicately interfingers unit tAa; it fills long, narrow,

shallow valleys, which implies a low emplacement viscosity for unit fsAb. A northwest-trending scarp forms the transition between unit tAa and fcAb where a distinct flow in unit fcAb, apparently sourced near the scarp, extends approximately 200 km toward feature *TMa*. Northwest-trending fractures located northeast of unit fsAb cut a radial fracture suite. Widely spaced (tens of kilometers) arcuate fractures to the northeast define a circle centered approximately on unit fsAb.

Feature *TMc* (C1 of Hansen [2002]) is defined by radial fractures that trace back to the low-backscatter material of unit fsAc (flows and shield-related material c of Artemis). Unit fsAc hosts numerous small shield edifices and interfingers with unit tAa; it fills long, narrow, shallow valleys, which implies low viscosity during emplacement. The penetrative fabric of unit tAa trends northwest and parallels a suite of quasi-radial fractures. Three moderately sized (tens of km) volcanic edifices lie to the north of feature *TMc* on unit tAa. The flows of composite unit fcAb fan away from feature *TMc* and locally cover the tectonic fabric of unit tAa.

Feature *TMd* (C5 of Hansen [2002]—the northeast-trending deformation belt of Brown and Grimm [1995] and the northeastern interior deformation belt of Spencer [2001]) dominantly consists of sub-parallel northeast-trending rounded ridges and flow-filled valleys. Feature *TMd* lies predominantly in unit tAb (tectonic terrain of Artemis, unit b), which grades into the adjacent unit tAa. Units tAb and tAa differ in radar brightness; unit tAa shows higher radar backscatter. Broad ridges parallel, and preserve, the penetrative fabric. Brown and Grimm (1995) identified northeast-trending flat-topped ridges, which they interpreted as a horst and graben. We did not observe flat-topped northeast-trending ridges in this area; in contrast we observed rounded ridges and angular peaked ridges. This discrepancy in observations likely arises from angular ridges appearing as flat-topped ridges due to radar image artifacts of the "magic airbrush" technique used by Brown and Grimm (1995). Northwest-trending fractures, scarps, and penetrative fabric in the northern part of feature *TMd* cut northeast-trending penetrative tectonic fabrics. Northwest-trending fractures in the southern part of feature *TMd* cut northeast-trending penetrative fabric. Roughly concentric fractures and scarps, which lie to the west of feature *TMd*, also cut the penetrative tectonic fabric and ridges. This region deserves detailed geologic mapping outside the limits of the current study; locally clear, but complex, cross-cutting relationships likely exist among the several tectonic elements; it appears however, that layer extension likely dominates the local tectonic story, as suggested within the published record (Brown and Grimm, 1995; Spencer, 2001). Ivne, a possible impact crater (see "Impact Crater" section for discussion), lies within feature *TMd*.

Britomartic Chasma trends northeast across the northern interior. Britomartic Chasma differs from most other chasmata on Venus in that it is <1,000 km in length, is not associated with an obvious corona chain (for example, Diana-Dali Chasmata, Hecata and Parga Chasmata), and is marked by smooth fold-like ridges (and troughs) rather than chasma-parallel fractures (for example, Diana-Dali Chasmata [Hansen and DeShon, 2002], Jana, Kuanja and Ralkumgu Chasmata [Bleamaster and Hansen, 2005], Devan Chasma [V–41 and V–29]). Britomartic Chasma hosts local flow units, and it fills local topographic valleys, as previously noted (see Brown and Grimm, 1995; Spencer, 2001; Hansen, 2002).

Penetrative Tectonic Fabric

A remarkably extensive penetrative tectonic fabric occurs within the stratigraphically lowest terrains of Artemis' interior. The fabric consists of tightly spaced lineaments (fig. 5). The lineaments display a generally consistent northeast trend; however, locally lineaments change trend in apparent spatial association with local tectonomagmatic centers (fig. 2, on map sheet). SAR images provide clues about the cross-sectional topographic shape of the penetrative fabric and therefore fabric morphology. The fabric has a gradational backscatter character across strike in both left- and right-illumination SAR imagery; this observation leads to the interpretation that the cross-sectional topography is generally marked by smooth, likely symmetric, ridges and troughs. Low-amplitude rounded ridges best fit the observations, although fracture-like topographic expressions and ambiguous topographic expressions also occur. Penetrative fabric wavelength is generally consistent across Artemis based on detailed transect measurements at 19 locations shown on the geologic map (table 2). Fabric wavelength, determined along transects normal to lineament trend, was determined using SAR images stretched to enhance the difference between light and dark lineaments, and represent maximum values because the ridges approach the effective resolution (Zimbelman, 2001) for the penetrative fabric using *Magellan* full-resolution SAR data. Wavelength ranges from 300–950 m (540±160m average). Ignoring one high outlier yields a range of 300–730 m (520±125 m average). The penetrative fabric was lumped together with other units as part of a single radar facies unit, radar-bright facies, which extended across the exterior, chasma, and interior regions (Hansen, 2002); it was part of the 'fine-scale fabric' unit occurring within both Artemis Chasma and the interior (Brown and Grimm, 1995). Herein, the penetrative fabric is delineated as a distinctive tectonic fabric marked by a short-wavelength fabric, which is penetrative at effective resolution.

The penetrative fabric primarily occurs in units tAa and tAb, however it locally extends into adjacent units. Penetrative fabric mapped outside of units tAa and tAb always occurs at gradational contacts determined primarily by a gradual decrease in radar backscatter character; fabric-parallel lineaments remain easily identifiable but appear slightly subdued. The subdued appearance may reflect weathering, varying degrees of burial by thin flows or aeolian fines, and/or reactivation of buried fabric structures. Low-backscatter material delicately interfingers with the penetrative fabric locally; this relation indicates that the low-backscatter material constitutes a thin veneer, marked by low viscosity during its emplacement, as would be required to fill the long, narrow, and shallow valleys without completely burying the penetrative fabric. The low-backscatter material is interpreted as consisting of local volcanic deposits. A sedimentary origin is unlikely owing to the present lack of significant erosion rates on Venus and the pristine appearance of adjacent rocks (and lack of evidence for erosion or dissection)

that would be the most probable source of sediment. In addition, a sedimentary origin might be expected to be less sensitive to local topography. Penetrative fabric-parallel lineaments in the low-backscatter material likely reflect the reactivation of buried penetrative fabric structures. The nature of the penetrative fabric is worth considering further, given its distinctive character and extensive regional development across much of Artemis Chasma's interior.

The morphologic characteristics of the penetrative fabric, summarized here, might provide clues to its formation, which could, in turn, impose constraints for models of Artemis' evolution. Penetrative fabric morphology (1) consists of symmetric(?) ridges with short wavelength (520±125 m), (2) shows relatively consistent along-strike character across the interior, (3) does not seem to be associated with parallel long-wavelength topography (and similarly lacks periodically spaced gaps), and (4) is developed across much of Artemis' interior, yet it has not been recognized within the chasma or exterior region. Observation 4 indicates that either (a) the penetrative fabric formed across the region and has been subsequently covered within the chasma and exterior (and therefore embodies temporal implications) or (b) penetrative fabric formation was limited to the interior, and thus does not carry direct temporal implications with regard to interior-chasma formation. Given (1) the lack of evidence for burial and embayment within the chasma, (2) temporal relations implied by unit fcAa and shallow troughs, which extend from the interior across the chasma to the exterior, and (3) buttressing relations that indicate broadly synchronous evolution of interior flows and chasma structures, we favor the hypothesis that penetrative fabric formation was limited to the interior of Artemis.

The fabric could record deformation of a pre-existing layer, in which case the fabric wavelength would likely reflect layer strength. It this case layer thickness would be 1 to 6 times wavelength (see Lan and Huddleston, 1995), or approximately 0.3 to 5 km, using average wavelength. It is difficult to envision a layer this thin across the entire interior of Artemis without associated longer wavelength features, indicating the presence of a strong subsurface support layer. In addition, the generally consistent northeast-trend of the fabric might have formed approximately normal to major layer shortening (if lineaments mark fold or thrust fault ridges) or extension (if lineaments represent fractures or normal faults), yet shortening or extension across an existing layer should lead to changes in layer thickness, and therefore the existence of multiple wavelengths. Furthermore, southeast-northwest shortening or extension of a pre-existing layer is difficult to reconcile with the rest of Artemis Chasma's geometry.

The physical nature of a laterally extensive, thin, relatively strong layer is difficult to address. A compositional difference between layers might provide one explanation. A compositional difference would require a mechanism to emplace a relatively uniform and thin layer of material across a very large area. Widespread sedimentation analogous to terrestrial ocean basin accumulation is one possibility. This would require liquid water to enhance erosion rates to create and transport sediment. Venus' surface presently lacks liquid water and significant erosion (Kaula, 1990). However, conditions on Venus could have been very different in the past. The high deuterium/hydrogen ratio of Venus' atmosphere is consistent with past wet conditions (Donahue, 1999), which may have supported widespread erosion and deposition.

Flood-lava flows might also create a thin layer with a different composition than subsurface material. This would require widespread volcanism across the entire interior of Artemis Chasma, low-viscosity lava, and presumably magma storage across a large area. The presence of a large subsurface magma chamber might be expressed by variation in the local strain regime; however, the penetrative fabric is moderately consistent in character and orientation across the entire interior, in apparent contradiction with predictions. Numerous small magma chambers or point sources of magma distributed across Artemis could provide source material with less influence on the local accumulation of strain. It is possible and even likely that the development of penetrative fabric and later tectonic deformation overprinted the surface expression of the magma chambers. However, the challenge remains—that is, how to impart a relatively coherent tectonic fabric upon this layer developed across Artemis Chasma's interior.

Alternatively, a rheologically defined thin layer might result from a locally elevated geothermal gradient that raises the regional brittle-ductile transition to shallow levels. Heating the shallow crust to high temperatures without melting could anneal the surface layer with time and thereby strengthen the layer. An elevated geothermal gradient might not result in a sharp décollement between a thin surface layer and the subsurface, however the importance of the width of this mechanical transition zone is unknown and a wider zone might be acceptable at the first order. Furthermore, this scenario retains the problem of the lack of a second long-wavelength fabric that might be expected as a result of a subsurface layer. In addition, recent finite-element modeling of short-wavelength folding by contracting and cooling of ultra-dry diabase at surface temperatures temporarily elevated to 1,000 K indicate that the high temperatures might threaten the competence of the thin layer, making formation and preservation of short-wavelength structures difficult (Ghent and others, 2005). However, the composition of Venusian crust is not well understood and could be much stronger, or weaker, than currently believed.

Another possibility is that Artemis' penetrative fabric formed progressively as the 'layer' itself formed, much like the fabric that characterizes terrestrial ocean crust parallel to, and observed along, submarine spreading centers. Indeed Artemis' penetrative fabric appears morphologically similar to surfaces along terrestrial mid-ocean ridges viewed in high-resolution shaded relief maps posted on the Ridge Multibeam Synthesis (RMBS) Data Portal website (fig. 6). The terrestrial RMBS shaded relief maps and Venusian SAR images might be comparable in that they each provide views of the detailed topographic character of planet surfaces. Unfortunately high-resolution views of this distinctive terrestrial tectonic fabric are not available across large regional areas away from the ridge axes; this lack of availability makes regional comparison with Artemis' penetrative fabric difficult. Despite this shortcoming, we favor formation of Artemis' penetrative fabric in a manner similar to terrestrial spreading center fabric herein—that is, marking the formation of new crust, with cross-strike time-transgressive

evolution. In this case Artemis' penetrative fabric would not mark deformation of a previously existing layer (hence a secondary tectonic fabric), but rather it would reflect the formation of crust, and as such, the penetrative fabric might more correctly be considered a primary tectonic fabric that formed with the evolution/emplacement of the material unit/crust. Within the context of this scenario, the layer need only be thin at the location of its formation, and it could thicken from below as a result of under-plating, as the surface/crust translates away from the spreading center with the formation of new crust, as is the case for Earth's oceanic crust.

Artemis' interior penetrative fabric shows a regionally coherent trend, yet it is also characterized by local variation, which might be similar to variations observed in high-resolution shaded- relief images of mid-ocean ridge fabrics. Within the southwestern interior of Artemis, the penetrative fabric is marked by a somewhat curvilinear fabric (fig. 7, on map sheet) in which the fabric locally deviates along parallel northwest-trending linear zones, and along one sharply defined zone in particular. Brown and Grimm (1995) originally proposed this sharp boundary as a dextral shear zone that displaces pre-existing lineaments in a right-lateral fashion. Given that the boundary coincides with a steep topographic slope, the apparent deflection of lineaments could be a result of radar foreshortening. Radar foreshortening would displace areas of high topography (in this case, the north side of the slope break) toward the direction of the radar, resulting in an *apparent*, but not real, change in trend. That is, the apparent bend in lineaments at this location might be best interpreted as a radar image artifact, rather than indicative of strike-parallel displacement. The oblique nature of the lineaments within the zone (as observed in high-resolution SAR data) suggests that the deflections are probably not solely artifacts. If the deflections are not solely artifacts of radar imaging, then it is important to know both the relative timing of the lineaments, as well as the nature of the lineaments—whether formed by shear, shortening, or extension processes—to constrain robust kinematic interpretations. The fabric is deflected in an apparent left-lateral sense along gentle slopes assuming that the fabric is simply sheared across the northwest-trending zone. However, if the penetrative fabric marks fold crests, the asymmetric fabric might record distributed sinistral, rather than dextral shear. If the penetrative lineaments mark extensional structures, then the region might record distributed northwest-southeast extension with distributed dextral (right-lateral) shear. The current data do not allow us to robustly and uniquely define either the nature of the lineament fabrics or their relative timing. Furthermore, comparison with terrestrial mid-ocean ridge fabrics and transform fault fabrics indicate that a specific kinematic interpretation might be suspect. We suggest here, however, that the interior penetrative fabric might be similar to terrestrial mid-ocean ridge fabrics, and it might record distributed extension that resulted in fabric and layer formation as well as lateral displacement (perhaps dextral in some places and sinistral at others) along sharp to distributed 'transform-like' zones. Within the context of this interpretation, the penetrative fabric would form generally perpendicular to the direction of extension (parallel to spreading center ridge trends). This suggestion should be treated as a working hypothesis and should be subject to scrutiny with further study using new and existing data. None of the scenarios outlined above can be eliminated with any certainty using currently available data, and other scenarios might indeed exist. Future missions with higher resolution imagery and topography data will help refine constraints on the penetrative fabric; stricter constraints might pose requirements that better constrain the possible options. Lander missions that provide geochemical data could also be helpful if the geologic context of their sampling is well constrained and understood. Detailed high-resolution structural mapping and analysis of the penetrative fabric might also provide critical clues to the formation of this distinctive fabric. Such a study is beyond the scope of this report. We favor the interpretation that Artemis' penetrative fabric is analogous to terrestrial mid-ocean ridge fabrics, and similarly reflects time-transgressive formation of new crust in a cross-strike (or high angle to strike) direction. The consideration of time-transgressive formation of this fabric, as opposed to formation indicative of a singular geologic 'event,' will play a critical role in understanding Artemis formation and, as such, has implications for Venusian geodynamics.

Temporal Relations and Geologic History

Few units or structures occur within each of the three Artemis regions: exterior, chasma, and interior; yet it appears that at least parts of each of these regions record a shared history. Artemis suites of tectonic structures at all scales show a remarkable consistency in style and trend. Suites of chasma-parallel structures, radial fractures, and wrinkle ridges each define individual circles each with their centers near the center of Artemis. Hansen (2002) suggested that these geometric relations are strongly suggestive of a genetic relationship; we concur with that interpretation, as we find no evidence to contradict this premise based on geometry and spatial relations. Thus, at the heart of our analysis is an acceptance that Artemis likely formed as a tectonically coherent entity with interior, chasma, and exterior regions evolving broadly contemporaneously. For this discussion, we depart from our earlier organization and discuss features from the interior of Artemis outward.

Artemis' interior units roughly divide into two groups. One group consists of radar-rough tectonic terrains (units tAa and tAb). The other group consists of radar-smooth (volcanic?) flow materials (units fcAa, fcAb, fsAa, fsAb, fsAc, fu, and flu). The penetrative tectonic fabric that marks units tAa and tAb shows a regionally consistent northeast trend throughout the interior. Radial and concentric structural suites and associated flows define four centers of tectonic and magmatic activity. Penetrative fabric typically marks the basal exposed terrain at most locations. Accordingly, although the onset of penetrative fabric formation is unconstrained, penetrative fabric formation appears to have formed (locally) relatively early in Artemis' interior history. However, this theory does not require that the penetrative fabric formed within a single geologic instant,

but rather, could record a time-transgressive process, just as terrestrial ocean crust forms time-transgressively. Penetrative fabric formation seems most likely to have involved the (progressive) creation of a layer across much (and perhaps all) of Artemis' interior. Penetrative fabric formation overlapped in time and space with tectonism of units tAa and tAb, and with the formation of the four tectonomagmatic centers (*TMa–d*). Cross-cutting relations suggest that the development of penetrative fabric broadly ended earlier (locally) than the development of the tectonomagmatic centers, or temporally overlapped with early stages of tectonomagmatic center evolution. We envision that the penetrative fabric records formation of new crust along a northeast-trend, with local modification of the crust at each of the tectonomagmatic centers.

Within Artemis' interior each of the four tectonomagmatic features (*TMa–d*) preserve histories of locally centralized deformation and volcanism. Evolution of the four centers broadly overlapped in time, and in concert with, though generally later than, the formation of local penetrative fabric elements. All four centers preserve histories that temporally and spatially overlap between centers. Flows that emanated from feature *TMa* cover flows that emanated from feature *TMb*, and vice versa, indicating broadly contemporaneous evolution of these two centers. The flows also locally bury pre-existing structures related to tectonomagmatic center formation. Lineaments in the flows show similar trends to those in the penetrative fabric; these lineaments likely represent reactivation of penetrative fabric structures. Flows in unit fcAb, located between features *TMc* and *TMd*, are difficult to individually delineate, and thus, to attribute to one tectonomagmatic center over the other. Additionally, flows in unit fcAb appear to emanate from feature *TMb* and flow toward feature *TMc*, and vice versa; however, no discrete boundary exists between opposing flows, which appear to laterally grade into each other. We interpret these relations as evidence of broadly synchronous and time-transgressive emplacement of these units at the scale of our analysis. Based on the surface record, the bulk of the deformation associated with tectonomagmatic centers predated the bulk of composite flow formation (or at least the flows preserved at the surface). Because observations are limited to the surface, we have no record of earlier (now subsurface) flows, which is a limitation of the data. Shield fields at the centers of features *TMa*, *TMb*, and *TMc* (units fsAa, fsAb, and fsAc, respectively) locally bury pre-existing structures related to their respective tectonomagmatic center, and these shields are in turn deformed by structures of the same trend and character that they bury. These relations indicate that the bulk of the individual shield fields' formation occurred as tectonomagmatic center deformation and evolution waned. No clear temporal relations exist between the evolution of the shield fields and the composite flows because these map units are not in contact with one another, and such relations would be below the resolution of the current SAR data.

The pervasive development of Artemis Chasma topography and chasma structures currently prohibits obvious correlations of interior units to exterior units. The evolution of individual tectonomagmatic centers can be related to other parts of Artemis' evolution. Unit fcAa extends from the interior (*TMa*) westward across Artemis Chasma and to the exterior. Shallow troughs, secondary structures associated with this flow unit, also extend from the interior to the exterior along Artemis' western boundary. We interpret that the flow unit and shallow troughs formed time-transgressively as flows covered trough and trough-cut flows, as also noted by Hansen (2002). In addition, the shallow troughs appear to both cut, and be cut by, chasma-parallel folds (fig. 8, on map sheet). We interpret these relations to indicate broadly contemporaneous, time-transgressive formation of both shallow troughs and chasma folds (and by association, the chasma trough). Unfortunately it is difficult to track individual shallow troughs across the chasma due to alternating left- and right-look SAR data at a high angle to shallow troughs and broadly parallel to the chasma and chasma structures. Local minor apparent right-lateral offset of the some shallow troughs likely reflects shortening across the chasma structures rather than true dextral translation; however some component of dextral displacement is certainly possible. The relations across the western part of Artemis trough indicate that feature *TMa* evolved time-transgressively and broadly contemporaneous with the formation of the western part of the chasma. In addition, the chasma records moderate, but not extreme, shortening across itself or its' interior; furthermore, no significant chasma-parallel translation is evident [or is recorded] across the chasma. The flows and fractures could have formed broadly prior to the chasma, and the chasma could have formed a topographic trough late during evolution of flows and fractures. There is no evidence that flows spilled into the topographic trough that marks the chasma. Along the eastern part of Artemis' interior, flows associated with *TMb* and *TMc* appear to locally embay chasma-related topography being buttressed by chasma-parallel folds at the boundary between the interior and Artemis Chasma. Some chasma-parallel structures near impact crater Behn cut unit fcAb, whereas other chasma-parallel structures in the area appear locally embayed by unit fcAb. These relations are consistent with broadly contemporaneous formation of the chasma structures and the emplacement of unit fcAb, which forms a composite, and likely time-transgressive, unit. Along the outer part of the eastern chasma (at about 3:00), exterior (radial) fractures are affected by chasma-parallel folds; crosscutting relations clearly indicate that the exterior fractures predated the formation of the outermost folds within Artemis Chasma (Brown and Grimm, 1995; Hansen, 2002, fig. 5 therein). These relations indicate that these radial fractures formed early with respect to chasma folds (and presumably chasma topography) at this location. Similar crosscutting relations occur within the southern part of Artemis Chasma, with exterior fractures locally preserved along the fold crests that lie within the outer parts of the chasma. There is no evidence that fractures occur within the inner parts of the chasma or its structures. It is unclear whether the fractures simply did not initially extend farther inward, or if the fractures have been obliterated either as a result of tectonic activity or burial. Given that no obvious flooding relations occur within Artemis Chasma, burial seems unlikely. We favor the interpretation that the fractures did not originally extend inward, but disruption by chasma tectonism is possible.

Fundamentally, the current resolution of the data does not place temporal constraints on the formation of the geologic units (materials) relative to the chasma (a topographic feature).

There are no units that appear to clearly flow into the topographic trough that marks the chasma, so all that can be stated, with guarded confidence, is that it is unlikely that the interior tectonomagmatic centers formed well after Artemis Chasma marked its current topography. We postulate that Artemis Chasma could have developed locally after flows associated with the various tectonomagmatic centers were emplaced, and that the chasma may have formed by local down warping of the surface; the trough could translate spatially in a direction normal to its trend.

As noted previously, structural suites that characterize the exterior region of Artemis—concentric wrinkle ridges and radial fractures—share a center point with Artemis Chasma, located within Artemis' interior region. We interpret these shared geometries as consistent with the suggestion that these exterior structures and Artemis Chasma are genetically related. The northeast-trending fracture zone abuts Artemis Chasma at approximately 7:00 to 8:00. Artemis Chasma, defined here both topographically and structurally, appears to narrow slightly, and to bend to the northeast along this juncture with the exterior northeast-trending fractures zone; these relations could indicate that the fracture zone and chasma might have formed over the same time interval. In any case, the fracture zone neither obviously cuts the chasma, nor does the chasma obviously cut the fracture zone. We suggest that the fracture zone and chasma might have evolved broadly synchronously, although we certainly cannot prove such a suggestion. The suggested timing relations are consistent with the current data. If Artemis Chasma served as a buttress to the younger propagation of the fracture zone, then we might expect to see evidence that the fracture zone, with a width of >200 km at the juncture, disrupted the chasma and chasma structures. If Artemis Chasma completely post-dated formation of the fracture zone we might expect to see a sharp difference in chasma structures at the juncture—which is not observed. Thus the slight narrowing of Artemis Chasma, and general lack of obvious crosscutting structural relations at the juncture of the chasma and the fracture zone suggest broadly contemporaneous evolution of the chasma and the fracture zone. It is also notable that the maximum extension direction across the chasma (northwest-southeast) broadly parallels the interpreted extension direction recorded by the interior penetrative fabric. Thus, we submit that the exterior fracture zone, the interior penetrative fabric, and the chasma might have evolved in broad temporal concert with one another, with the difference in interior penetrative fabric and exterior fracture zone perhaps reflecting marked differences in crustal rheology on either side of the evolving Artemis Chasma.

The eastern corona chain with Teteoinnon Corona marking the final feature barely extends into the V–48 quadrangle. Temporal relations between the corona chain in general, and Teteoinnon Corona, specifically with Artemis, are unconstrained.

Hypothesis Evaluation

Four hypotheses have been proposed for Artemis' formation: subduction, metamorphic core complex, bolide impact, and deep mantle plume (fig. 9, on map sheet). Each hypothesis is discussed briefly and evaluated based on constraints gleaned from this 1:5 million-scale geologic mapping effort.

Subduction Hypothesis

The subduction hypothesis highlights the cross-strike topographic similarity of Artemis Chasma to terrestrial subduction trenches (McKenzie and others, 1992; Brown and Grimm, 1995; Schubert and Sandwell, 1995; Brown and Grimm, 1996). The subduction hypothesis suggests that northwest-directed convergence resulted in under thrusting of approximately 250 km of 'lower-plate' exterior lowlands (from the southeast) beneath what is now Artemis' interior (*upper plate*). If the postulated subducted slab lacked water for magmatic fluxing (for example, Kaula, 1990), then slab subduction would be expected to contribute to local *depression* of the regional geothermal gradient above the slab resulting in a lack of *upper plate* volcanic activity, as favored by proponents of the subduction hypothesis. If sufficient water existed (consistent with, but not required by, atmospheric isotopic data; for example, Donahue and Russell, 1997; Donahue and others, 1997; Donahue, 1999; Lecuyer and others, 2000; Hunten, 2002) and lead to magmatic fluxing, then upper plate volcanism might be expected to result in an alignment of volcanic features above the proposed subducted slab that formed concurrently with upper-plate tectonism. Thus volcanic activity within the interior of Artemis would either predate chasma formation (dry), or form as a result of subduction (wet). Either way, within the context of the subduction hypothesis, topographic expression of Artemis Chasma would result from flexure of the down-going slab, represented by the exterior lowland. However, flexure does not appear to be an adequate explanation for the topographic expression of the entire chasma in plan view. Plates should slip past each other rather than over or under ride one another where their common boundary is sub-parallel to the direction of convergence. Accordingly, flexure should not occur where the chasma axis trends generally northwest or southeast. Anticipating this, yet favoring the subduction hypothesis, Brown and Grimm (1995; 1996) suggested that Artemis Chasma actually represents three distinct trough segments. One is the part of the chasma from approximately 2:30 to 6:30 that denotes a subduction zone marked by approximately 250 km of under-thrusting of exterior lowlands to the southeast under Artemis' interior. The second is the chasma segment from 12:00 to 2:30 that marks an associated trough dominated by focused left-lateral displacement (a sort of transform plate boundary). The third segment is the chasma between 6:30 and 10:30 that corresponds to an older feature, genetically unrelated to the other two segments. In this scenario the chasma never existed between 10:30 and 12:00, which is consistent with geologic relations.

The subduction hypothesis embodies several predictions that can be evaluated based on the results of geologic mapping. The first prediction is that the southwest part of the trough formed prior to, and is unrelated to, the northeast-southeast segment. This prediction is contradicted by temporal relations that suggest the chasma formed as a coherent feature as evi-

denced by the marked continuity of chasma parallel structures along the entire trace of the chasma, as well as near orthogonal fractures. A second prediction is that the chasma segment from 6:30 and 10:30 should record right-lateral displacement that accompanied postulated northwest-directed subduction along the chasma segment from 2:30 to 6:30. In detail there is no evidence for focused right-lateral displacement across the chasma, and, in fact, shallow troughs cross the chasma along the southwest boundary with broadly overlapping temporal relations with chasma structures (fig. 8, on map sheet). The local minor apparent right-lateral offset of the some shallow troughs likely reflects shortening across the chasma structures rather than true dextral translation. The low amount of possible dextral offset falls far short of the 250 km of displacement predicted. In addition, Brown and Grimm (1995) also interpreted right-lateral shear in a northwest-trending deformation belt at the southwest margin of feature *TMa*, which lies within the interior (and therefore the postulated upper-plate) rather than within the chasma, and yet might have accompanied subduction zone formation. It is unclear what a dextral shear interpretation is based upon, and as noted previously, kinematic implications of real or apparent deflections of the lineaments deflections are debatable. The third prediction is that section of the chasma from 12:00 to 2:30 should record structural fabrics indicative of left-lateral displacement. However, Hansen (2002) found no evidence for sinistral displacement, nor did the current study reveal evidence for the required kinematic picture.) A fourth prediction is that interior volcanism should pre-date chasma formation (subduction hypothesis proponents call for dry Venusian conditions), yet temporal relations seem more consistent with contemporaneous development of the chasma and interior volcanism. Composite flow unit fcAa, interpreted herein as genetically related to feature *TMa*, extends across the western margin of the chasma. Cross-cutting relations are consistent with broadly contemporaneous formation of feature *TMa* and at least a part of Artemis Chasma. In addition, unit fcAb, interpreted herein as genetically related to features *TMb* and *TMc*, appears to embay chasma-related structures along parts of the inner southeastern chasma margin; chasma-parallel lineaments, near impact crater Behn, also deform unit fcAb and yet also variably display evidence of burial by unit fcAb. In addition, small chasma-parallel ridges in unit fcAb near the southeast margin may represent inversion structures (for example, DeShon and others, 2000; Hansen, 2005) or reactivation of buried fractures. These relations indicate that the interior volcanic activity temporally overlapped to some extent with formation of the chasma, at least at these locations. A fifth prediction is that chasma-concentric normal faults might be expected to form in the outer rise out board of the chasma segment from approximately 2:30 to 6:30. However, no normal faults are documented, and instead, wrinkle ridges—indicative of distributed layer contraction—form concentric to, and out board of, the chasma. Flexural modeling obtained reasonable fits for this southeastern part of Artemis Chasma, although it required a high in-plane force to prevent brittle failure in the outer rise (Brown and Grimm, 1996).

Each of these observations taken together with documented continuity of structures along the entire trough in a trough-parallel fashion clockwise from 12:00 to 10:30, and a shared central location of trough topography, trough structures, radial fractures and wrinkle ridges, support the interpretation that the various features of Artemis are genetically related. In addition to map relations, the angle of subduction required by the tight curvature of Artemis trough is not geometrically viable on a planet the size of Venus. If subduction did occur along the length of Artemis Chasma, the *lower plate* must have deformed in a cylinder-like fashion, or the plate would emerge on the northwest side of Artemis. We find no compelling evidence for either scenario. And even if we did find evidence supportive of either scenario, neither situation would constitute subduction.

Metamorphic Core Complex Hypothesis

The metamorphic core complex hypothesis suggests that Artemis records a composite structure in which the interior represents a metamorphic core complex that resulted from exposure of crust deformed in a ductile manner (Spencer, 2001). Spencer (2001) postulated that the center of Artemis represents the grooved surface of a 300-km-square molded footwall of a crustal extensional system exposing deep crustal rocks due to approximately 170 km of northwest-southeast directed extension. The northern interior part of Artemis would represent *lower plate* deep crustal rocks marked by ductile northwest-trending grooves formed as a result of plastic molding of the footwall by irregularities on the underside of the hanging wall. Despite a rather detailed and restrictive interpretation of specific structures, the metamorphic core complex hypothesis is not comprehensive. It does not place postulated crustal extension into a regional context, and it makes very few testable predictions. In addition, the lack of significant erosion on the surface of Venus (Arvidson and others, 1992) makes exhumation of deep crustal rocks unlikely and proves challenging for the metamorphic core complex hypothesis. On Earth, significant crustal extension can result in the translation of deep crustal rocks to shallow crustal levels; but erosion processes expose those rocks at the surface. Rocks that record ductile deformation can also become exposed as a result of extension along terrestrial spreading centers, although extension associated with spreading also requires recycling of other crust at subduction zones. Spencer (2001) does not suggest how analogous recycling might be accommodated on Venus. The metamorphic core complex hypothesis does not address the formation of: (1) the tectonomagmatic centers, (2) the interior penetrative fabric (which trends perpendicular to the predicted ductile elongation tectonic fabric), (3) Artemis Chasma, or (4) the concentric outer high. As proposed, the metamorphic core complex hypothesis is essentially untestable owing to lack of details.

Bolide Impact Hypothesis

The bolide impact hypothesis suggests that Artemis marks the surface expression of a huge bolide impact that formed on a cold, solid Venus, no later than 3.9 Ga (Hamilton, 2005). The impact hypothesis makes few specific predictions about Artemis' morphology, structures, or possible related volcanic activ-

ity; as such, the bolide impact hypothesis requires speculation on many important details. Furthermore, the impact hypothesis does not address many first-order aspects of Artemis including topography and geologic relations, nor does it consider studies of large impact features and expected morphological features. Artemis' topographic form, with a narrow (100–150 km) circular trough surrounding a raised interior, is opposite that of large impact basins on Mars and the Moon, which display circular rims surrounding huge interior basins. For example, Mars' Hellas Planitia, widely accepted as impact in origin, forms a 2,000-km diameter, 6–8 km deep, circular basin surrounded by a modified outer rim (fig. 10, on map sheet). Hamilton (2005) infers that when Artemis formed, early Venus would have been rheologically similar to Mars during the formation of the Hellas impact basin. Therefore, within the context of the impact hypothesis, these two huge impact features (Artemis and Hellas) should show similar first-order character. Although Venus and Mars differ geologically, huge impact basins on both planets, as well as on Earth, should be negative topographic features unless strong geophysical or rheological reasons suggest otherwise (see Jones and others, 2005). Models of large bolide impact that result in massive partial melting of the mantle and possible formation of interior highs require thin lithosphere (~10 km or less; allowing the bolide to penetrate the crust) (for example, Jones and others, 2005; Elkins-Tanton and Hager, 2005). Large impact basins commonly show multiple- ring morphology (Wilhelms, 1973; Hartmann, 1998), and Artemis lacks such morphology. In addition, contrary to the assertion by Hamilton (2005), there is no evidence that a northwest part of Artemis Chasma (10:30 to 12:00) is buried beneath other constructs (Brown and Grimm, 1995, 1996; Hansen, 2002; this study). Results presented herein indicate that Artemis Chasma narrows and shallows tracing clockwise from the southeast; chasma-related structures fade along the chasma with the diminishing topographic expression. We found no evidence of embayment of the chasma structures within this region, which would be expected in the case of burial. Additionally, the interaction of shallow troughs and chasma lineaments do not show any obvious strain partitioning or deflection that might be expected if a significant crustal anisotropy such as a buried chasma were present. Accordingly, there is no evidence that Artemis Chasma once formed a complete circular trough that experienced late burial along its northwest trace. Finally, the impact hypothesis does not address the formation of the interior tectonomagmatic features or formation of the penetrative tectonic fabric developed across the interior, despite the hypothesis inference that Artemis represents a coherent set of features formed within a very short geologic timeframe.

The bolide impact hypothesis is currently poorly developed and lacks such salient predictions as: (1) the size of bolide, (2) the thickness and rheology of the lithosphere at time of impact (except that the lithosphere was 'cold' and hence thick), (3) specific structures and structural patterns associated with large bolide impact, or (4) possible role of impact-induced melting. The bolide impact hypothesis does not address many first-order observations including: (1) Artemis topography, (2) the lack of a complete circular feature, (3) formation of interior tectonomagmatic centers, or (4) formation of the interior penetrative fabric with a regionally consistent northeast-trend. If significant impact melt were generated during Artemis' formation by bolide impact, then a thin mechanical layer might have formed (although it is not clear how this could happen), and perhaps a penetrative fabric could develop (for example, Hansen, 2006). However, the consistent northeast structural trend would not be predicted, and it is difficult to reconcile with the bolide impact hypothesis. Ultimately the bolide impact hypothesis, as published, is not a viable explanation for the formation of Artemis Chasma and would require further development in light of the geologic constraints presented herein as well as elsewhere in the literature.

Plume Hypothesis

The plume hypothesis suggests that Artemis represents the surface expression of a deep mantle plume (Griffiths and Campbell, 1991; Smrekar and Stofan, 1997; Hansen, 2002, 2007). This hypothesis initially arose from laboratory plume experiments aimed at modeling the interaction of a thermally driven mantle plume with the lithosphere (Griffiths and Campbell, 1991), and from later numerical modeling aimed at modeling corona formation (Smrekar and Stofan, 1997). Both physical and numerical models resulted in the formation of a circular trough, postulated as analogous to Artemis Chasma. Griffiths and Campbell (1991) also noticed that their physical plume experiments developed small-scale convection cells that compartmentalized the interior of the flattening plume head. The tectonomagmatic centers might represent subsurface compartmentalization contributing to the evolution of Artemis' interior region. As an alternative to small-scale thermally driven convection cells, Hansen (2002) proposed the formation of compositionally driven diapirs above a flattening plume head to accommodate formation of the localized tectonomagmatic centers in Artemis' interior. The formation of Artemis' interior tectonomagmatic centers as diapirs is consistent with numerical modeling of diapirs (for example, Koch and Manga, 1996; Smrekar and Stofan, 1997). The plume hypothesis also accommodates crustal heterogeneity, which could influence strain partitioning and prevent map patterns idealized from physical and numerical models from developing.

Within the context of the plume hypothesis, Artemis' topography should reflect a raised interior region, consistent with the observed topography of a raised interior region surrounded by a 1- to 2-km-deep chasma. Furthermore Artemis Chasma would have formed a coherent entity broadly synchronous with interior volcanic deposits and deformation, and deformation in the exterior. This prediction is consistent with the continuity of chasma structures, radial fractures and concentric exterior wrinkle ridges that strongly suggest a genetic relationship and broadly contemporaneous formation. As noted above, interior deformation and volcanic deposits formed broadly synchronously with the chasma.

The interpretation that Artemis represents the surface manifestation of a mantle plume on thin lithosphere, is consistent with Artemis' large size and circular planform. Gravity-topography analysis, though not unique, is consistent with at

least partial dynamic support for Artemis (Simons and others, 1997). However, contemporary dynamic support requires a contemporary age for Artemis—a prediction that we can neither support nor reject based on currently available data. As a deep-mantle plume rises toward the lithosphere, the lithosphere will be uplifted, and, if the strength of the lithosphere is exceeded, radial fractures could form above the plume head. An alternate scenario is if the lithosphere were sufficiently heated it might develop a penetrative tectonic fabric. A circular trough could also form, as illustrated in laboratory experiments aimed at modeling the interaction of thermal plumes with the lithosphere (Griffiths and Campbell, 1991). In Griffiths and Campbell's (1991) experiments, as a plume head approached the rigid horizontal boundary, it collapsed and spread laterally. A layer of surrounding 'mantle,' squeezed between the plume and the surface, resulted in a gravitationally trapped asymmetric instability, and this process led to the formation of an axisymmetric trough. In addition, the interior squeezed layer might lead to convection on a scale much smaller than that of the original plume. These smaller scale instabilities could interact with the lithosphere inside the trough, and become manifested as the tectonomagmatic centers. It was on the basis of these laboratory experiments that a plume model for Artemis formation was proposed following initial release of Magellan SAR data (Griffiths and Campbell, 1991). Finite-element models of the interaction of a large thermal plume with lithosphere, aimed at modeling corona topography, also show development of an axisymmetric trough above large thermal mantle plumes (Smrekar and Stofan, 1997). In this case the trough results from delamination of the lower lithosphere. Delamination might contribute to a hybrid model that incorporates aspects of plume-lithosphere interactions with signatures that some workers propose might be better addressed through subduction, although subduction vergence might differ.

A Hybrid Hypothesis

Although the plume hypothesis seems the most consistent with geologic relations, it does not address the formation of the penetrative fabric. We suggest a hybrid hypothesis that builds on the plume hypothesis, but which might incorporate aspects of each of the four existing hypotheses. The hypothesis embodies two important postulates. One is that Artemis represents a singular geomorphic-tectonomagmatic feature, and, as such, the interior, chasma, and exterior evolved together. A second postulate is that various parts of Artemis formed transgressively, both spatially and temporally. We suggest that Artemis marks the surface expression of a large mantle plume that emerged within a broad mantle upwelling; the interaction of the upwelling, the plume, and the lithosphere resulted in significant rheological differences across the exterior, interior, and chasma regions. The exterior preserves a distal record of the initial plume-lithosphere interactions, as reflected in radial and concentric structures; the interior records the formation of new crust at a terrestrial-like spreading center and associated tectonomagmatic activity during plume evolution; the chasma preserves parts of crust modified directly above the plume early in plume-lithosphere interactions, and subsequently shortened during the evolution of the plume. A series of time-step cartoons illustrates salient features of this new hypothesis, beginning with the arrival of a deep mantle plume at the base of relatively thin lithosphere (fig. 11, on map sheet). Part of the crust resides above a broad quasi-cylindrical mantle upwelling (marked by the exterior fracture zone) where the crust is thinned, thermally and/or mechanically, relative to its global counter part (fig. 11, time 0). With arrival of the plume, the lithosphere/crust was uplifted due to thermal buoyancy, resulting in the formation of radial fractures and concentric wrinkle ridges, now preserved in the region outside Artemis Chasma (which forms later). The area above the plume thins (light-gray region forming the interior of Artemis to be), and there is a fundamental rheological boundary between the interior crust affect by the plume, and exterior crust, which lay outside the spatial limits of thermal-rheological influence of the plume. As the plume head flattens and spreads the plume tail delivers hot mafic magma to the surface, forming a nascent spreading center, also likely fed by pressure-release melting in the mantle (time 2); the penetrative fabric preserves a record of this newly formed crust, geomorphically similar to the crust formed at terrestrial mid-ocean ridges. With time, the 'spreading center' propagates along strike, influenced by both the plume and the broad mantle-upwelling (time 3). As new crust forms at the spreading center the previously formed crust is displaced outward from the spreading center; a trough develops within the modified crust (light gray), possibly along its boundary with the newly formed crust, marked by penetrative fabric. The trough moves outward with continued spreading and propagation of the spreading center, which propagates parallel to the trend of the broad mantle upwelling. The translation is driven both by spreading and new crust formation at the surface, and dynamics at the plume-lithosphere interface (from below; as in the case of laboratory experiments). Tectonomagmatic centers form locally within the region thinned by initial plume-lithosphere interaction (time 4, time 5), presumably as a result of localized magmatic activity related to the plume. Once the thinned/modified crust and the newly formed crust (marked by the penetrative fabric) meet the relatively unmodified crust (that region exterior to the current chasma), the trough (chasma) can no longer move outward as the crustal rheology is simply too strong and resists deformation (time 6). Spreading need not have occurred at a single spreading center, but rather could have occurred across various parts of Artemis' interior.

Within the context of this hybrid hypothesis the interior, exterior, and chasma formed as genetically related features, each evolving through time, and related to the evolution of a plume-lithosphere interaction. The plume's interaction with the lithosphere (or lack thereof) would account for strong rheological variation at a crustal-scale across the region as shown in figure 11 (on map sheet). The exterior fracture zone abuts the chasma as a result of rheological factors, with fracture zone and chasma evolving synchronously. The trough (chasma) represents a sort of nascent, but failed, subduction zone with the exterior region lying within an *upper plate* position relative to the interior *lower plate*. This proposal differs from the subduction hypothesis, which calls for northwest-directed subduction of the lowland under the Artemis interior (which would lie in an *upper plate* position). The hypothesis differs from the

metamorphic core complex hypothesis in that interior extension results in the formation of new crust, rather than the exposure of mid- to deep-level crust within Artemis' interior. The hybrid hypothesis is similar to each of these in that it calls for shortening of the surface crust within Artemis Chasma—which moves outward with time. And it calls for northwest-southeast directed extension across the interior of Artemis. With regard to the third hypothesis, it is possible that the mantle plume formed in response to a large bolide (>20–30 km diameter) impact on thin lithosphere, with the interior region representing a region of greatly thinned and modified crust as a result of the impact event and subsequent massive partial melting in the mantle (for example, Jones and others, 2005; Elkins-Tanton and Hager, 2005). In this case the plume called for in time steps 1–6, could have formed in response to large bolide impact with a thin global lithosphere (for example, Wichman and Schultz, 1995), rather than the result of strictly endogenic processes. At this point we cannot favor plume formation via one mechanism over another (for example, endogenic rise of a deep mantle plume, or in response to an exogenic catastrophe); however, a thin lithosphere would be required in either case.

Several relations fall out of the hybrid hypothesis. (1) The exterior fracture zone and the interior region of Artemis formed broadly synchronously, although they developed quite different characteristics due to both different rheological characters and different spatial locations within the postulated tectonic framework. (2) Artemis Chasma could have moved outward through time; as such, the chasma topography could modify features previously formed at the surface. The chasma might move in a fashion similar to the ring-trough observed in experiments (for example, Griffiths and Campbell, 1991), and the subsurface delamination front developed in numerical models (Smrekar and Stofan, 1997). Artemis' structures, volcanic units, and topography each record complex (but predictable) temporal relationships with one another. Within the context of the hybrid hypothesis, structures (and surface units) could both predate and postdate the formation of the trough, which would actually change spatial location (and size) through time. (3) Artemis Chasma might be somewhat akin to terrestrial subduction zones in that it marks a zone of shortening, however, the proposed vergence would vary from the published subduction hypothesis in that the exterior region would form the *upper plate* whereas the interior region, marked by newer crust and penetrative fabric, would form the *lower plate*. (4) Artemis might represent Venus' failed attempt to develop plate-tectonic processes. (5) Reasons that Artemis may have failed to develop into a divergent plate boundary (along the nascent spreading center) and subduction zone (Artemis Chasma) could be a function of the lithospheric strength, perhaps tied specifically to the postulated rheological profile of dry versus wet lithosphere (for example, Regenauer-Lieb and others, 2001). Venus' crust is currently dry and strong (Mackwell and others, 1998), which might have rendered its lithosphere too strong for the nascent spreading center to propagate outside the region of lithosphere modified above the plume head. In addition, water might play a critical role in subduction initiation (and hence plate tectonics) due to the mode of failure of silicate lithospheres (Regenauer-Lieb and others, 2001). Convergence across a dry lithosphere (such as Venus) results in focused brittle failure of the upper lithosphere, while the bottom of the lithosphere deforms in a diffuse fashion; the bottom of the lithosphere delaminates and recycles to the mantle—leaving the surface crust relatively intact. In contrast, wet lithosphere (as is the case on Earth) fails across its entire mechanical thickness, resulting in the formation of a narrow fault-like zone through the lithosphere; in this case the entire lithospheric thickness recycles to the mantle (Regenauer-Lieb and others, 2001). Once initiated, subduction of the entire lithosphere could provide a means of recycling water to the mantle, triggering a double feedback mechanism (thermoelastic and thermal-rheological) to promote plate tectonics (Regenauer-Lieb and others, 2001). In the case of a dry lithosphere (Venus), any surface water or hydrated surface crust would remain at the surface, and water would not be returned to the mantle.

At this point in the study of Artemis, it seems to us most likely that Artemis resulted, at some first-order level, from the interaction of a deep mantle plume with relatively thin lithosphere, along the lines outlined above. Clearly there is room for much discussion and debate about the formation of Artemis. There is also room for numerous additional studies of this wonderfully puzzling circular feature. High-resolution geologic mapping of existing datasets, as well as new even higher resolution datasets will shed much new information on the detailed character of Artemis' surface features, as well as on the temporal and rheological evolution of the various surfaces. Such studies will provide critical clues to Artemis' formation and evolution and the operative dynamic processes responsible for the formation of this apparently unique tectonic feature.

The current 1:5 million-scale geologic map does not provide enough detail to determine how Artemis formed with significant confidence, and it thus remains an unexplained feature. Did the unique morphology of Artemis result from serendipitous formation from the spatial and temporal overlap of genetically unrelated events or processes? Does Artemis' unique character call for a unique process, or a relatively common process active under unique (rheological) conditions? Or does Artemis record a relatively unique (rheological) time in the evolution of this dynamic planet? Settling on a single hypothesis for the formation of Artemis seems premature at this time; it is entirely possible that the most likely mode of Artemis' formation has not yet been put forward.

References Cited

Addington, E.A., 2001, A stratigraphic study of small volcano clusters on Venus: Icarus, v. 149, p. 16–36.

Arvidson, R.E., Greeley, R., Malin, M.C., Saunders, R.S., Izenberg, N., Plaut, J.J., Stofan, E.R., and Shepard, M.K., 1992, Surface modification of Venus as inferred from Magellan observation of plains: Journal of Geophysical Research, v. 97, p. 13,303–13,318.

Baker, V.R., Komatsu, G., Gulick, V.C., and Parker, T.J., 1997, Channels and valleys, *in* Bouger, S.W., Hunten, D.M., and Phillips, R.J., eds., Venus II, University of Arizona Press, p. 757–798.

Baker, V.R., Komatsu, G., Parker, T.J., Gulick, V.C., Kargel, J. S., and Lewis, J.S., 1992, Channels and Valleys on Venus—Preliminary analysis of Magellan data, Journal of Geophysical Research, v. 97, p. 13,395–13,420.

Banerdt, W.B., McGill, G.E., and Zuber, M.T., 1997, Plains tectonics on Venus, *in* Bouger, S.W., Hunten, D.M., and Phillips, R.J., eds., Venus II: Tucson, University of Arizona Press, p. 901–930.

Barsukov, V.L., Basilevsky, A.T., Kuzmin, R.O., Pronin, A.A., Kryuchkov, V.P., Nikolayeva, O.K., Chernaya, I.M., Burba, G.A., Borbina, N.N., Sashkina, V.P., Markov, M.S., and Sukhanov, A.L., 1984, Geology of Venus from the result of analysis of radar images taken by Venera 15/16 probes—Preliminary data: Geochimica, v. 12, p. 1,811–1,820.

Barsukov, V.L., Basilevsky, A.T., Burba, G.A., Bobinna, N.N., Kryuchkov, V.P., Kuzmin, R.O., Nikolaeva, O.V., Pronin, A.A., Ronca, L.B., Chernaya, I.M., Shashkina, V.P., Garanin, A.V., Kushky, E.R., Markov, M.S., Sukhanov, A.L., Kotelnikov, V.A., Rzhiga, O.N., Petrov, G.M., Alexandrov, Y.N., Sidorenko, A.I., Bogomolov, A.F., Skrypnik, G.I., Bergman, M.Y., Kudrin, L.V., Bokshtein, I.M., Kronrod, M.A., Chochia, P.A., Tyuflin, Y.S., Kadnichansky, S.A., and Akim, E.L., 1986, The Geology and Geomorphology of the Venus surface as revealed by the radar images obtained by Veneras 15 and 16: Journal of Geophysical Research, v. 91, p. D378–D398.

Basilevsky, A.T., Ivanov, B.A., Burba, G.A., Chernaya, I.M., Kryuchkov, V.P., Nikolaeva, O.V., Campbell, D.B., and Ronca, L.B., 1987, Impact craters of Venus—A continuation of the analysis of data from the Venera 15 and 16 Spacecraft, Journal of Geophysical Research, v. 92, no. 12, p. 12,869–12,901.

Bleamaster, L.F., II, and Hansen, V.L., 2005, Geologic map of the Ovda Regio quadrangle (V–35), Venus: U.S. Geological Survey Geologic Investigations Series I–2808, scale 1:5,000,000, 1 plate.

Bouger, S.W., Hunten, D.M., and Phillips, R.J., 1997, Venus II: Geology, geophysics, atmosphere, and solar wind environment: Tucson, University of Arizona Press, p. 1362.

Brown, C.D., and Grimm, R.E., 1995, Tectonics of Artemis Chasma: a Venusian "plate" boundary: Icarus, v. 117, p. 219–249.

Brown, C.D., and Grimm, R.E., 1996, Lithospheric rheology and flexure at Artemis Chasma, Venus: Journal of Geophysical Research, v. 101, no. 5, p. 12,697–12,708.

Bussey, D.B.J., Sorensen, S.-A., and Guest, J.E., 1995, Factors influencing the capability of lava to erode its substrate—Application to Venus: Journal of Geophysical Research, v. 100, no. 8, p. 6,941–6,949.

Campbell, B.A., 1999, Surface formation rates and impact crater densities on Venus: Journal of Geophysical Research, v. 104, no. E9, p. 21,951–21,955.

Campbell, D.B., and Burns, B.A., 1979, Venus—Further evidence of impact cratering and tectonic activity from radar observations: Science, v. 204, p. 1,424–1,427.

Chapman, M.G., 1999, Geologic map of the Galindo quadrangle (V–40), Venus: U.S. Geological Survey Geologic Investigations Series I–2613, scale 1: 5,000,000.

Crumpler, L.S., Aubele, J.C., Senske, D.A., Keddie, S.T., Magee, K.P., and Head, J.W., 1997, Volcanoes and centers of volcanism on Venus, *in* Bouger, S.W., Hunten, D.M., and Phillips, R.J., eds., Venus II Geology, Geophysics, Atmosphere, and Solar Wind Environment: Tucson, The University of Arizona Press, p. 697–756.

DeLaughter, J.E., and Jurdy, D.M., 1999, Corona classification by evolutionary stage: Icarus, v. 139, no. 1, p. 81.

DeShon, H.R., Young, D.A., and Hansen, V.L., 2000, Geologic evolution of southern Rusalka Planitia, Venus: Journal of Geophysical Research, v. 105, p. 6,983–6,995.

Donahue, T.M., 1999, New analysis of hydrogen and deuterium escape from Venus: Icarus, v. 141, no. 2, p. 226.

Donahue, T.M., and Russell, C.T., 1997, The Venus atmosphere and ionosphere and their interaction with the solar wind—An overview, *in* Bouger, S.W., Hunten, D.M., and Phillips, R.J., eds., Venus II: Tucson, University of Arizona Press, p. 3–31.

Donahue, T.M., Grinspoon, D.H., Hartle, R.E., and Hodges, R.R., 1997, Ion/neutral escape of hydrogen and deuterium—Evolution of water, *in* Bouger, S.W., Hunten, D.M., and Phillips, R.J., eds., Venus II: Tucson, University of Arizona Press, p. 385–414.

Donahue, T.M., Hoffman, J.H., Hodges, R.R., Jr., and Watson, A.J., 1982, Venus was wet—A measurement of the ratio of deuterium to hydrogen: Science, v. 216, no. 4546, p. 630–633.

Elkins-Tanton, L., and Hager, B., 2005, Giant meteoroid impacts can cause volcanism: Earth and Planetary Science Letters, v. 239, p. 219–232.

Ferrill, D.A., Wyrick, D.Y., Morris, A.P., Sims, D.W., and Franklin, N.M., 2004, Dilational fault slip and pit chain formation on Mars: GSA Today, v. 14, no. 10, p. 1–9.

Ford, J.P., Plaut, J.J., Weitz, C.M., Farr, T.G., Senske, D.A., Stofan, E.R., Michaels, G., and Parker, T.J., 1993, Guide to Magellan Image Interpretation, National Aeronautics and Space Administration Jet Propulsion Laboratory Publication 93-24.

Ghent, R.R., Phillips, R.J., Hansen, V.L., and Nunes, D.C., 2005, Finite element modeling of short-wavelength folding on Venus—Implications for the plume hypothesis for crustal plateau formation: Journal of Geophysical Research-Planets, v. 110, no. E11, p. E11,006.

Greeley, R., 1987, Planetary Landscapes: London, Allen & Unwin, 275 p.

Gregg, T.K.P., and Greeley, R., 1993, Formation of venusian canali—Consideration of lava types and their thermal behaviors: Journal Geophysical Research, v. 98, no. E6, p. 10,873–10,882.

Grieve, R.A.F., and Head, J.W., 1981, Impact cratering, a geological process on the planets: Episodes, v. 4, no. 2, p. 3–9.

Griffiths, R.W., 1986a, Dynamics of mantle thermals with constant buoyancy or anomalous internal heating: Earth and Planetary Science Letters, v. 78, p. 435–446.

Griffiths, R.W., 1986b, The differing effects of compositional and thermal buoyancies on the evolution of mantle diapirs: Physics of the Earth and Planetary Interiors, v. 43, p. 261–273.

Griffiths, R.W., and Campbell, I.H., 1991, Interaction of mantle plume heads with the Earth's surface and onset of small-scale convection: Journal of Geophysical Research, v. 96, p. 18,295–18,310.
Grimm, R.E., and Hess, P.C., 1997, The crust of Venus, *in* Bouger, S.W., Hunten, D.M., and Phillips, R.J., eds., Venus II, Tuscon, University of Arizona Press, p. 1,205–1,244.
Guest, J.E., Bulmer, M.H., Aubele, J.C., Beratan, K., Greeley, R., Head, J.W., Micheals, G., Weitz, C., and Wiles, C., 1992, Small volcanic edifices and volcanism in the plains on Venus: Journal of Geophysical Research, v. 97, p. 15,949–15,966.
Hamilton, V.E., and Stofan, E.R., 1996, The geomorphology and evolution of Hecate Chasma, Venus: Icarus, v. 121, no. 1, p. 171–194.
Hamilton, W.B., 2005, Plumeless Venus has ancient impact-accretionary surface, *in* Foulger, G.R., Natland, J.H., Presnall, D.C., and Anderson, D.L., eds., Plates, Plumes, and Paradigms: Geological Society of America Special Paper Denver, Geological Society of America, p. 781–814.
Hansen, V.L., 2000, Geologic mapping of tectonic planets: Earth and Planetary Science Letters, v. 176, p. 527–542.
Hansen, V.L., 2002, Artemis: signature of a deep Venusian mantle plume: Geological Society of America Bulletin, v. 114, no. 7, p. 839–848.
Hansen, V.L., 2003, Venus diapirs; thermal or compositional?: Geological Society of America Bulletin, v. 115, no. 9, p. 1040–1052.
Hansen, V.L., 2005, Venus's shield terrain: Geological Society of America Bulletin, v. 117, no. 5/6, p. 808–820.
Hansen, V.L., 2006, Geologic constraints on crustal plateau surface histories, Venus: The lava pond and bolide impact hypotheses: Journal of Geophysical Research, v. 111, p E11,010.
Hansen, V.L., 2007, LIPs on Venus: Chemical Geology, v. 241, no. 3–4, p. 354–374.
Hansen, V.L., and DeShon, H.R., 2002, Geologic map of the Diana Chasma Quadrangle (V–37), Venus: U.S. Geological Survey Geologic Investigations Series I–2752, scale 1:5,000,000.
Hansen, V.L., Phillips, R.J., Willis, J.J., and Ghent, R.R., 2000, Structures in tessera terrain, Venus—Issues and answers: Journal of Geophysical Research, v. 105, p. 4,135–4,152.
Hartmann, W.K., 1998, Moons and Planets, Florence, Kentucky, Brooks Cole Publishing, 528 p.
Hauck, S.A., Phillips, R.J., and Price, M.H., 1998, Venus: Crater distribution and plains resurfacing models: Journal of Geophysical Research, v. 103, no. 6, p. 13,635–13,642.
Head, J.W., and Solomon, S.C., 1981, Tectonic evolution of the terrestrial planets: Science, v. 213, p. 62–76.
Herrick, R.R., Sharpton, V.L., Malin, M.C., Lyons, S.N., and Feely, K., 1997, Morphology and morphometry of impact craters, *in* Bouger, S.W., Hunten, D.M., and Phillips, R.J., eds., Venus II, Tucson, University of Arizona Press, p. 1,015–1,046.
Hunten, D.M., 2002, Exospheres and Planetary Escape, *in* Mendillo, M., Nagy, A., and Waite, J.H., eds., Atmospheres in the Solar System—Comparative Aeronomy: American Geophysical Union Monograph, p. 191–202.
Ivanov, M.A., and Head, J.W., 2003, Evolution of three largest coronae on Venus, Heng-O, Quetzalpetlatl, and Artemis—Preliminary Results [abs.], *in* Lunar and Planetary Science XXXIV, abstract 1188: Houston, Lunar and Planetary Institute, [CD-ROM].
Izenberg, N.R., Arvidson, R.E., and Phillips, R.J., 1994, Impact crater degradation on Venusian plains: Geophysical Research Letters, v. 21, p. 289–292.
Jones, A.P., and Pickering, K.T., 2003, Evidence for aqueous fluid-sediment transport and erosional processes on Venus: Journal of the Geological Society London, v. 160, p. 319–327.
Jones, A.P., Wunemann, K., and Price, D., 2005, Impact volcanism as a possible origin for the Ontong Java Plateau (OJP), *in* Foulger, G.R., Natland, J.H., Presnall, D.C., and Anderson, D.L., eds., Plates, plumes, and paradigms: Geological Society of America Special Paper, p. 711–720.
Kaula, W.M., 1990, Venus—A contrast in evolution to Earth: Science, v. 247, p. 1,191–1,196.
Kirk, R., Soderblom, L., and Lee, E., 1992, Enhanced visualization for interpretation of Magellan radar data—Supplement to the Magellan special issue: Journal of Geophysical Research, v. 97, p. 16,371–16,380.
Koch, D.M., and Manga, M., 1996, Neutrally buoyant diapirs—A model for Venus coronae: Geophysical Research Letters, v. 23, p. 225–228.
Komatsu, G., and Baker, V.R., 1994, Meander properties of Venusian channels: Geology, v. 22, no. 1, p. 67–70.
Lan, L., and Huddleston, P.J., 1995, The effects of rheology on the strain distribution in single layer buckle folds: Journal of Structural Geology, v. 17, no. 5, p. 727–738.
Lang, N.P., and Hansen, V.L., 2006, Venusian channel formation as a subsurface process: Journal of Geophysical Research-Planets, v. 111, no. E4, p. E04,001.
Lecuyer, C., Simon, L., and Guyot, F., 2000, Comparison of carbon, nitrogen and water budgets on Venus and the Earth: Earth and Planetary Science Letters, v. 181, p. 33–40.
Mackwell, S.J., Zimmerman, M.E., and Kohlstedt, D.L., 1998, High-temperature deformation of dry diabase with application to tectonics on Venus: Journal of Geophysical Research, v. 102, p. 975–984.
Masursky, H., Eliason, E., Ford, P.G., McGill, G.E., Pettengill, G.H., Schaber, G.G., and Schubert, G., 1980, Pioneer Venus radar results—Geology from images and altimetry: Journal of Geophysical Research, v. 85, p. 8232–8260.
McDaniel, K., and Hansen, V. L., 2005, Circular lows, a genetically distinct subset of coronae? [abs.]: Lunar and Planetary Science Conference, v. XXXVI, abstract 2367 [PDF].
McDaniel, K.M., 2005, Circular lows—A genetically distinct subset of coronae on Venus? Duluth, University of Minnesota, M.S. thesis, 79 p.
McKenzie, D., Ford, P.G., Johnson, C., Parsons, B., Sandwell, D., Saunders, S., and Solomon, S.C., 1992, Features on Venus generated by plate boundary processes: Journal of Geophysical Research, v. 97, no. E8, p. 13,533–13,544.
McKinnon, W.B., Zahnle, K.J., Ivanov, B.A., and Melosh, H.J.,

1997, Cratering on Venus—Models and observations, *in* Bouger, S.W., Hunten, D.M., and Phillips, R.J., eds., Venus II, Tucson, University of Arizona Press, p. 969–1014.
Nikolayeva, O.V., 1993, Largest impact features on Venus—Non-preserved or non-recognizable?: Lunar and Planetary Science Conference 24, p. 1,083–1,084.
Nikolayeva, O.V., Ronca, L.B., and Bazilevskiy, A.T., 1986, Circular structures on the plains of Venus as indicating geological history: Geochemistry International, v. 23, no. 9.
Nimmo, F., and McKenzie, D., 1998, Volcanism and tectonics on Venus: Annual Review of Earth and Planetary Sciences, v. 26, p. 23–51.
Okubo, C.H., and Martel, S.J., 1998, Pit crater formation on Kilauea volcano, Hawaii: Journal of Volcanology and Geothermal Research, v. 86, no. 14, p. 1–18.
Phillips, R.J., and Hansen, V.L., 1994, Tectonic and magmatic evolution of Venus: Annual Reviews of the Earth and Planetary Sciences, v. 22, p. 597–654.
Phillips, R.J., and Hansen, V.L., 1998, Geological evolution of Venus—Rises, plains, plumes and plateaus: Science, v. 279, p. 1,492–1,497.
Phillips, R.J., and Izenberg, N.R., 1995, Ejecta correlations with spatial crater density and Venus resurfacing history: Geophysical Research Letters, v. 22, no. 12, p. 1,517–1,520.
Plaut, J.J., 1993, Stereo imaging, *in* Ford, J.P., Plaut, J.J., Weitz, C.M., Farr, T.G., Senske, D.A., Stofan, E.R., Michaels, G., and Parker, T.J., eds., Guide to Magellan Image Interpretation, NASA Jet Propulsion Laboratory Publication 93-24, p. 33–41.
Regenauer-Lieb, K., Yuen, D.A., and Branlund, J., 2001, The initiation of subduction—Criticality by addition of water?: Science, v. 294, no. 5542, p. 578–580.
Roberts, K.M., and Head, J.W., 1993, Large-scale volcanism associated with coronae on Venus—Implications for formation and evolution: Geophysical Research Letters, v. 20, p. 1,111–1,114.
Rosenblatt, P., and Pinet, P.C., 1994, Comparative hypsometric analysis of Earth and Venus: Geophysical Research Letters, v. 21, p. 465–468.
Sandwell, D.T., and Schubert, G., 1992, Flexural ridges, trenches, and outer rises around coronae on Venus: Journal of Geophysical Research, v. 97, p. 16,069–16,084.
Saunders, R.S., Spear, A.J., Allin, P.C., Austin, R.S., Berman, A.L., Chandlee, R.C., Clark, J., deCharon, A.V., Jong, E.M.D., Griffith, D.G., Gunn, J.M., Hensley, S., Johnson, W.T.K., Kirby, C.E., Leung, K.S., Lyons, D.T., Michaels, G.A., Miller, J., Morris, R.B., Morrison, A.D., Piereson, R.G., Scott, J.F., Shaffer, S.J., Slonski, J.P., Stofan, E.R., Thompson, T.W., and Wall, S.D., 1992, Magellan Mission Summary: Journal of Geophysical Research, v. 97, p. 13,063–13,066.
Schaber, G.G., and Boyce, J.M., 1977, Probable distribution of large impact basins on Venus—comparison with Mercury and the Moon, *in* Roddy, D.J., Pepin, R.O., and Merrill, R.B., eds., Impact and explosion cratering—Planetary and terrestrial implications: New York, Pergamon Press, p. 603–612.
Schaber, G.G., Strom, R.G., Moore, H.J., Soderblom, L.A., Kirk, R.L., Chadwick, D.J., Dawson, D.D., Gaddis, L.R., Boyce, J.M., and Russell, J., 1992, Geology and distribution of impact craters on Venus: What are they telling us?: Journal of Geophysical Research, v. 97, p. 13,257–13,302.
Schubert, G., Moore, W.B., and Sandwell, D.T., 1994, Gravity over coronae and chasmata on Venus: Icarus, v. 112, no. 1, p. 130–146.
Schubert , G., and Sandwell, D.T., 1995, A global survey of possible subduction sites on Venus: Icarus, v. 117, p. 173–196.
Schultz, P.H., 1993, Searching for ancient Venus [abs.]: Lunar and Planetary Science, v. XXIV, p. 1,255.
Simons, M., Solomon, S.C., and Hager, B.H., 1997, Localization of gravity and topography: constraints on the tectonics and mantle dynamics of Venus: Geophysical Journal International, v. 131, no. 1, p. 24–44.
Smrekar, S.E., and Stofan, E.R., 1997, Corona formation and heat loss on Venus by coupled upwelling and delamination: Science, v. 277, no. 5330, p. 1,289–1,294.
Solomon, S.C., 1993, The geophysics of Venus: Physics Today, v. 46, no. 7, p. 48–55.
Solomon, S.C., Head, J.W., Kaula, W.M., McKenzie, D., Parsons, B., Phillips, R.J., Schubert, G., and Talwani, M., 1991, Venus tectonics—Initial analysis from Magellan: Science, v. 252, p. 297–312.
Spencer, J., 2001, Possible giant metamorphic core complex at the center of Artemis Corona, Venus: Geological Society of America Bulletin, v. 113, p. 333–345.
Squyres, S.W., Janes, D.M., Baer, G., Bindschadler, D.L., Schubert, G., Sharpton, V.L., and Stofan, E.R., 1992, The morphology and evolution of coronae on Venus: Journal of Geophysical Research, v. 97, p. 13,611–13,634.
Stofan, E.R., Hamilton, V.E., Janes, D.M., and Smrekar, S.E., 1997, Coronae on Venus—Morphology and origin, *in* Bouger, S.W., Hunten, D.M., and Phillips, R.J., eds., Venus II, Tucson, University of Arizona Press, p. 931–968.
Stofan, E.R., Senske, D.A., and Michaels, G., 1993, Tectonic features in Magellan data, *in* Ford, P. J., Plaut, J., Wietz, C. M., Farr, T. G., Senske, D. A., Stofan, E. R., Michaels, G., and Parker, T. J., eds., Guide to Magellan image interpretation, Pasedena, Calif., National Aeronautics and Space Administration Jet Propulsion Laboratory, p. 93–108.
Stofan, E.R., Sharpton, V.L., Schubert, G., Baer, G., Bindschadler, D.L., Janes, D.M., and Squyres, S.W., 1992, Global distribution and characteristics of coronae and related features on Venus—Implications for origin and relation to mantle processes: Journal of Geophysical Research, v. 97, p. 13,347–13,378.
Surkov, Y.A., Moskalyova, L.P., Kharyukova, V.P., Dudin, A.D., Smirnov, G.G., and Zaitseva, S.Y., 1986, Venus rock composition at the Vega-2 landing site: Journal of Geophysical Research, v. 91, no. B13, p. E215–E218.
Tanaka, K.L., compiler, 1994, The Venus geologic mappers' handbook, 2nd ed.: U.S. Geological Survey Open-File Report 94-438, 68 p.
Tanaka, K.L, Anderson, R.C., Dohm, J.M, Hansen, V.L., McGill, G.E., Schultz, R.A., Watters, T.R., 2010, Planetary

structural mapping—tectonics, *in* Schultz, R.A., and Watters, T.R., eds., Planetary Tectonics, Cambridge University Press, p. 351–396.

Vita-Finzi, C., Howarth, R.J., Tapper, S.W., and Robinson, C.A., 2005, Venusian craters, size distribution and the origin of coronae, *in* Foulger, G.R., Natland, J.H., Presnall, D.C., and Anderson, D.L., eds., Plates, plumes, and paradigms: Denver, Geological Society of America Special Paper 388, p. 815–824.

Wichman, R.W., and Schultz, P.H., 1995, Floor-fractured craters in Mare-Smythii and west of Oceanus-Procellarum—Implications of crater modification by viscous relaxation and igneous intrusion models: Journal of Geophysical Research, v. 100, no. E10, p. 21,201–21,218.

Wilhelms, D.E., 1973, Comparison of Martian and Lunar multiringed circular basins: Journal of Geophysical Research, v. 78, no. 20, p. 4,084–4,095.

Wilhelms, D.E., 1990, Geologic mapping, *in* Greeley, R., and Batson, R.M., eds., Planetary Mapping: London, Cambridge University Pres, p. 296.

Williams-Jones, G., Williams-Jones, A.E., and Stix, J., 1998, The nature and origin of Venusian canali: Journal of Geophysical Research, v. 103, no. 4, p. 8,545.

Zimbelman, J.R., 2001, Image resolution and evaluation of genetic hypotheses for planetary landscapes: Geomorphology, v. 37, no. 3–4, p. 179–199.

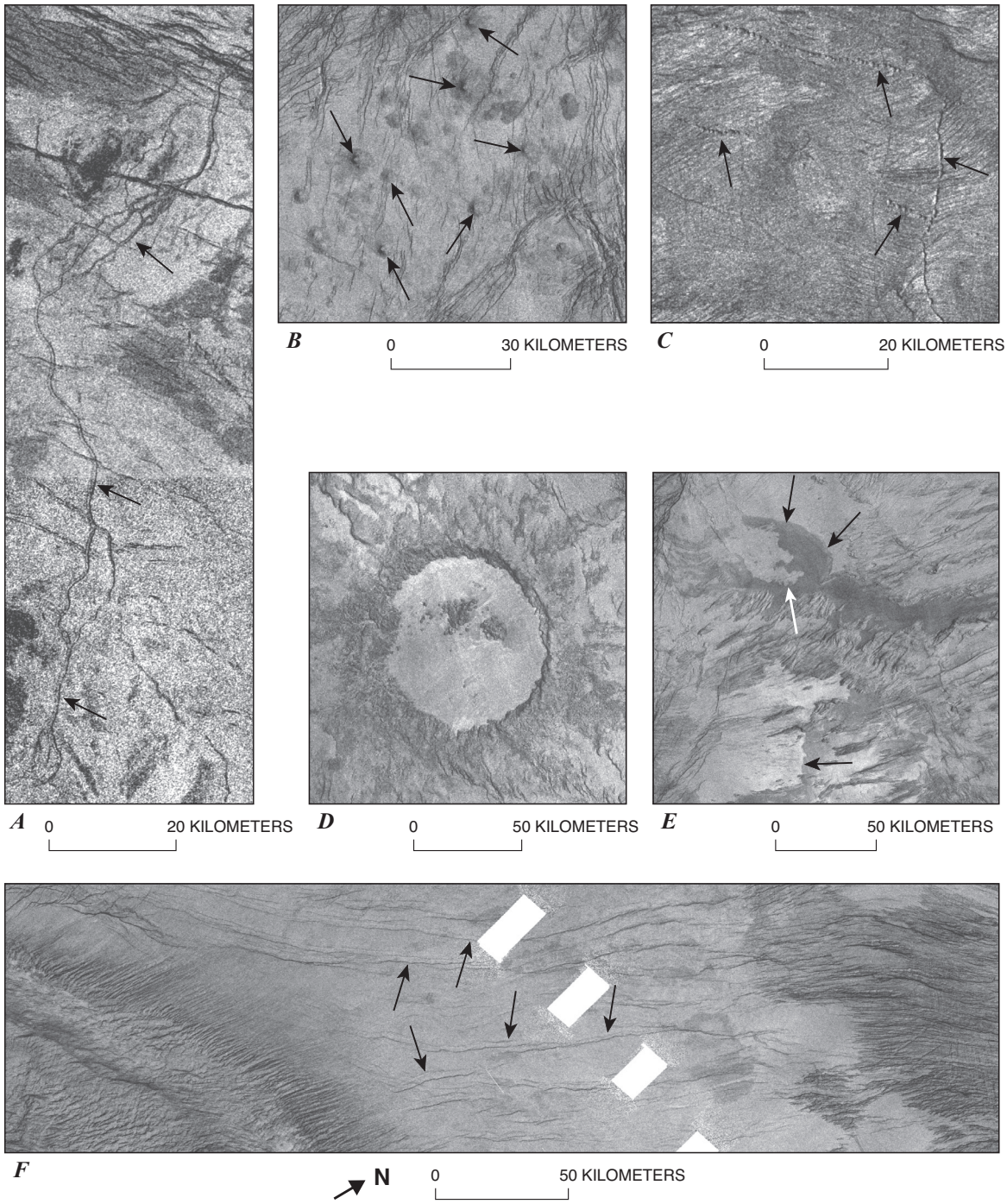

Figure 3. Examples of primary structures in V–48 (center coordinates): ***A***, channel (124°00' E., 25°07' S.); ***B***, shields (137°39' E., 32°43' S.); ***C***, pit chains (127°52' E., 26°09' S.); ***D***, impact crater (127°02'E, 36°04' S.); ***E***, flow fronts (133°11' E., 37°31' S.); and ***F***, shallow troughs (126°34' E., 31°46' S.). All images are left-look inverted SAR; white rectangles in image ***F*** are data gaps. North toward top of image, except where noted.

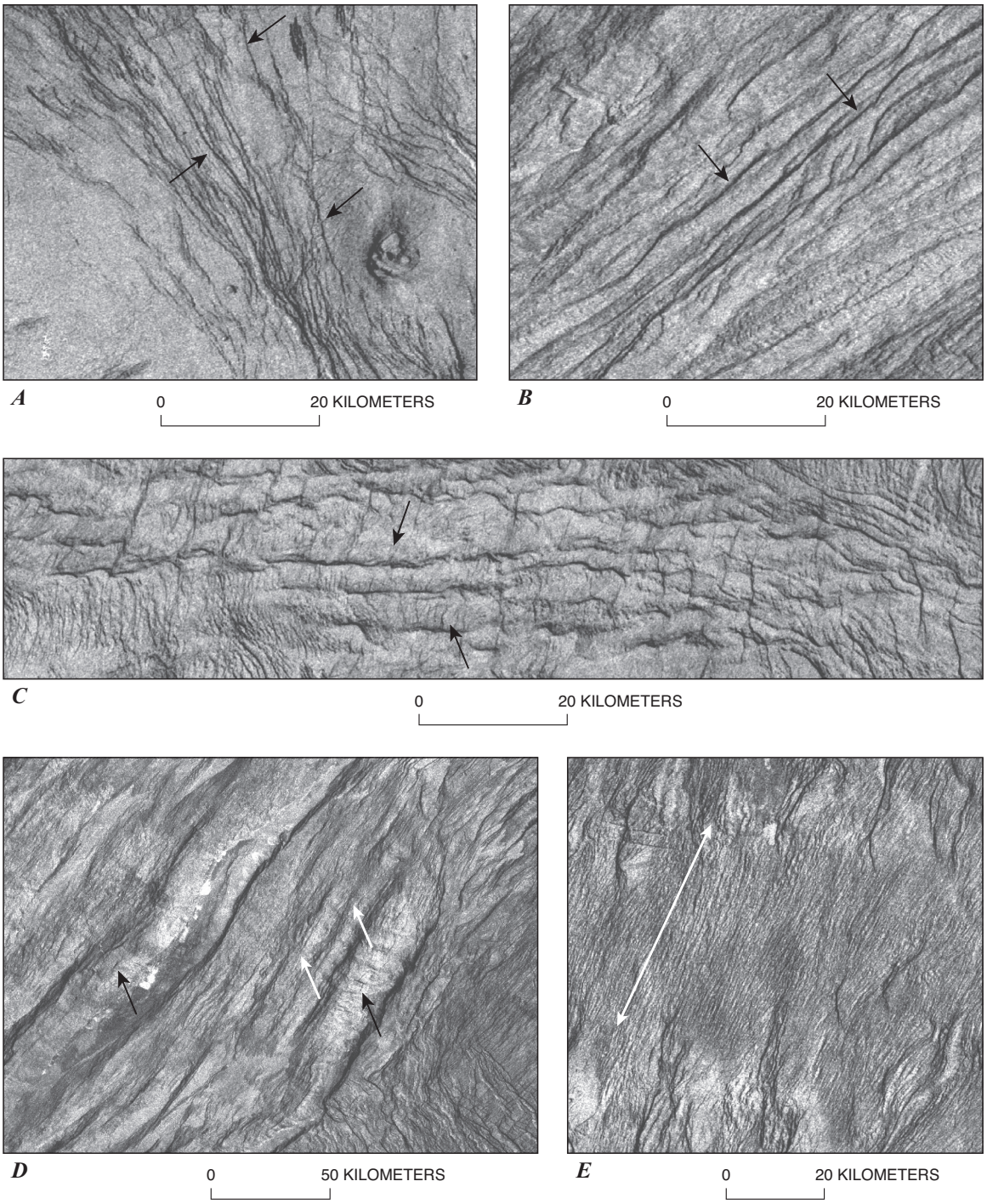

Figure 4. Examples of secondary structures in V–48 (center coordinates). ***A***, fractures (136°16' E., 36°59' S.); ***B***, lineaments (139°07' E., 40°58' S.); ***C***, folds (130°28' E., 34°36' S.); ***D***, ridges (134°32' E., 28°18' S.), black arrows point to large ridges, white arrows indicate small ridges; ***E***, penetrative fabric (130°20' E., 30°44' S.), white line with arrows parallels fabric trend. All images are inverted left-look SAR.

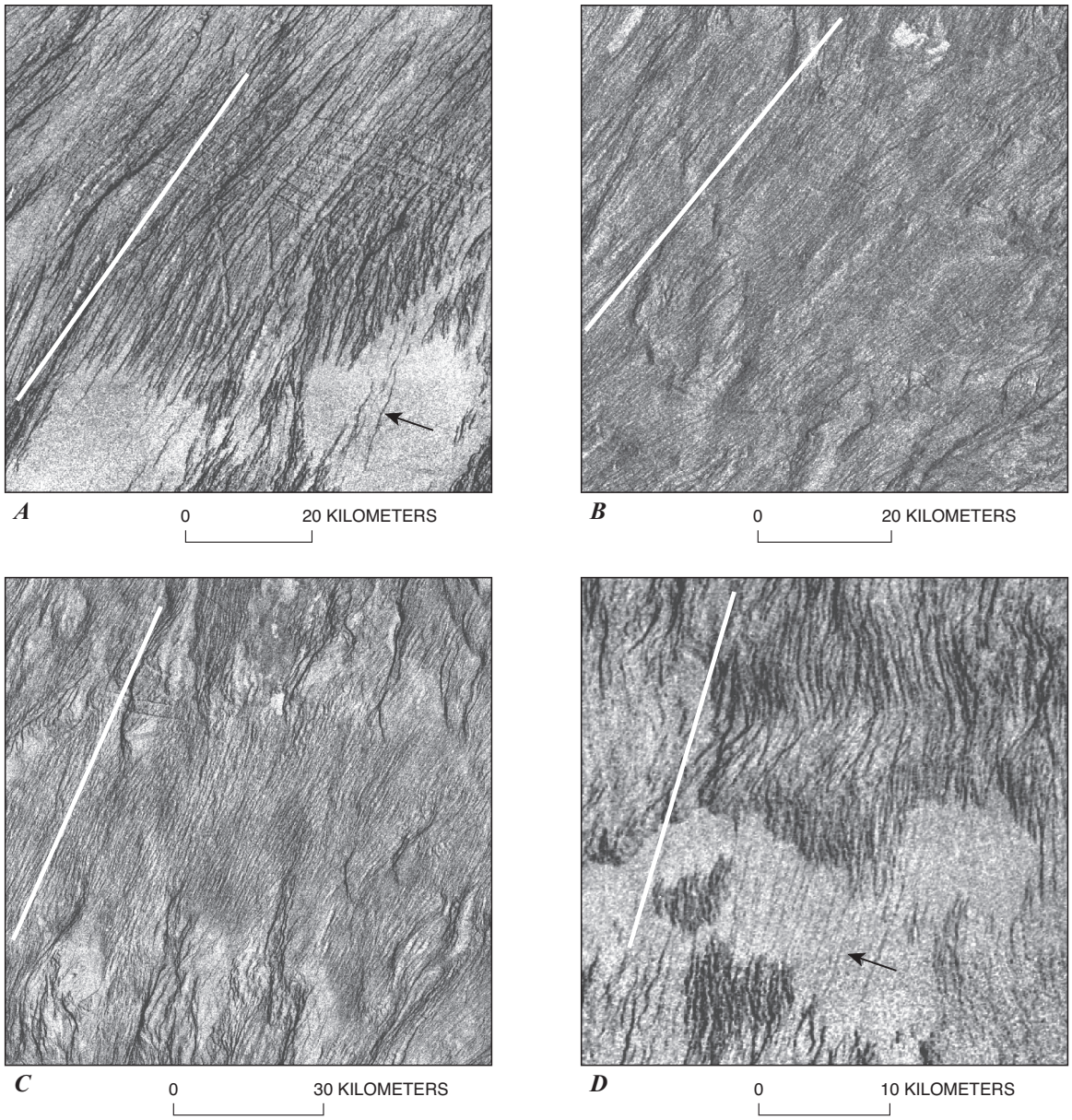

Figure 5. Representative inverted left-look SAR images of Artemis' penetrative fabric to indicate the range of character; white lines parallel fabric trend; (center coordinates): ***A***, (127°41' E., 30°38' S.); ***B***, (136°29' E., 27°59' S.); ***C***, (130°16' E., 30°42' S.); ***D***, (129°39' E., 32°38' S.). Fabric appears fracture-like in ***A*** and ***D***, and ridge-like in ***B*** and ***C*** (more common). Note the delicate interfingering of radar-smooth (light in color, low-backscatter) material with penetrative fabric (***A*** and ***D***) indicating: (1) the topographic expression associated with the penetrative fabric, (2) that the cover material forms a thin layer emplaced after fabric development, which (3) appears to have been low viscosity during emplacement; local cutting of the cover material by penetrative fabric trends likely represents reactivation of the buried penetrative fabric, and, in turn suggests that penetrative fabric structures were locally reactivated following the emplacement of the cover material.

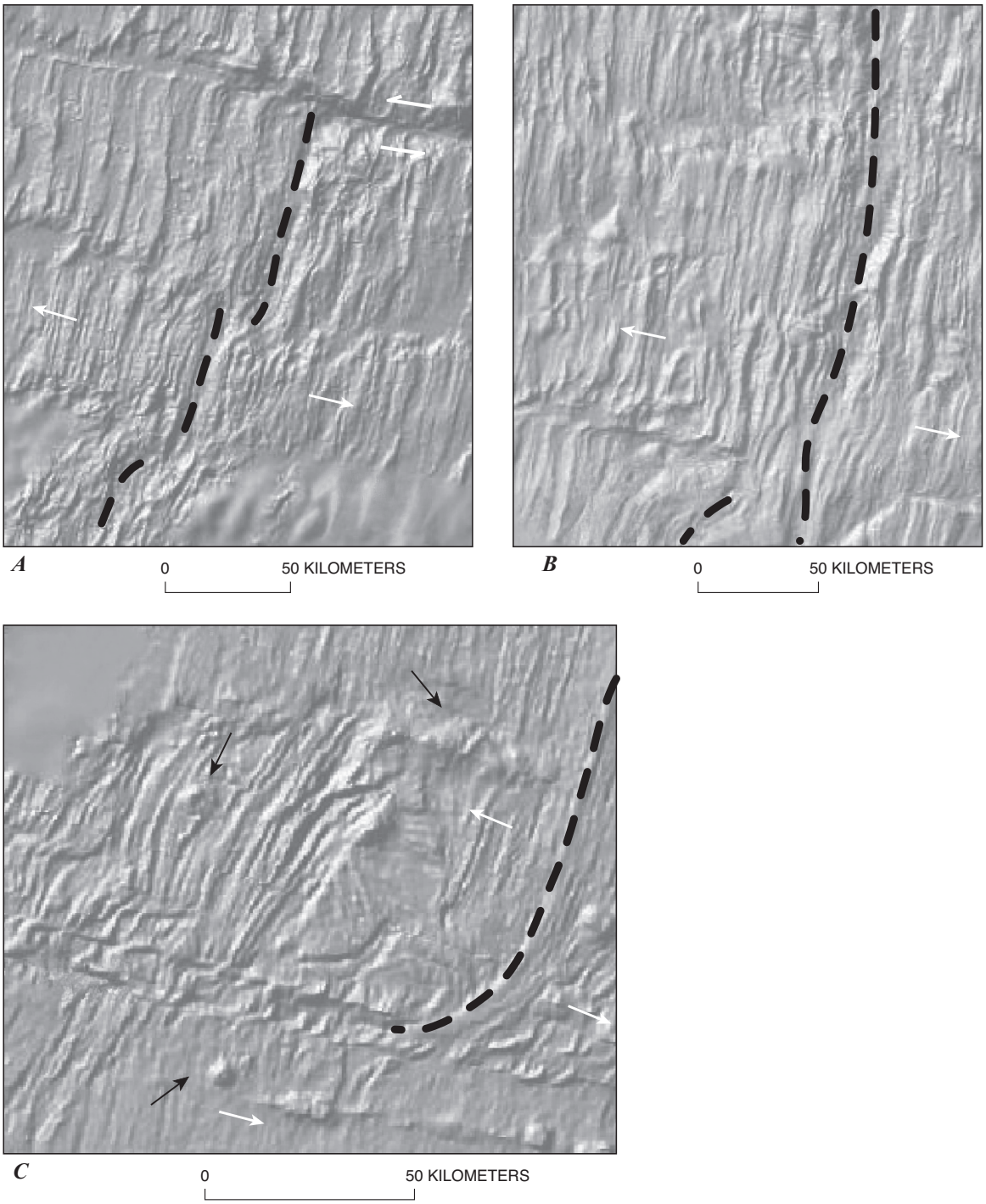

Figure 6. High-resolution shaded-relief images of terrestrial spreading centers from the Ridge Multibeam Synthesis (RMBS) Data Portal website (http://www.marine-geo.org/rmbs/). ***A***, A part of the northern Mid-Atlantic Ridge centered at 29°30’ N. and 43° W.; the ridge trough trends from the upper right to lower left, with a left-lateral transform fault to the right of the ridge trough and a fracture zone to the upper left. ***B***, A part of the northern Mid-Atlantic Ridge centered at 22°30’ N. and 45°30’ W.; the ridge trough trends NNE along the right side of the image. ***C***, A part of the southern East Pacific Rise centered at 8°50’ S. and 108°40’ W.; NNE-trending ridge lies along the right side of the image; a complex left-lateral transform zone trends WNW in the lower part of the image; volcanic constructs occur individually and as short chains. In each case high-resolution data exists only near the ridge axis. Ridge axes indicated by dashed black lines; volcanic constructs marked by black arrows; relative displacement across ridges and transform faults shown by white arrows. Compare with penetrative fabric in figures 5 and 6. For more images see website listed above.

Table 1. Crater data for the Artemis Chasma quadrangle (V–48), Venus.

Name	Latitude (° S)	Longitude (° E)	Diameter (km)	Unit location	Ejecta blanket	Impact halo	Central peak	Rim	Interior flooding	Modification	Crater density* (Herrick) /1x10^6 km^2
Behn	–32.4	142.0	25.8	fcAb	Y	N	Y	Y	Y	Fractured	1.91
Bonnevie	–36.1	127.0	87.6	tAa/fsAa	Y	Y	Y	Y	Y	Pristine	0.96
Ivne (crater?)	–27.0	132.8	9.0	tAb	Y	N	N	Y	?	Fractured	---
Jalgurik	–42.4	125.1	7.7	fu	Y	N	N	Y	N	Pristine	1.59
Janyl	–28.0	138.8	5.4	tAa/fcAb	Y	N	N	Y	N	Pristine	1.59
O'Connor	–26.0	143.9	29.6	fu	Y	N	Y	Y	Y	Pristine	2.55
Veronica	–38.1	124.6	17.9	tAa	Y	N	N	Y	Y	Fractured	1.27
Yomile	–27.3	138.7	13.6	tAa	Y	Y	N	Y	N?	Pristine	1.59
Unnamed	–41.56	142.9	4.5	tAa	Y	N	N	Y	N?	Pristine	---

*Crater density at a crater's location. Value is the density of craters represents the number of craters (including the specified crater) within a 1,000-km radius circle, and normalized to give the number of craters per 1 x 10^6 km^2

Table 2. Penetrative fabric wavelengths measured across Artemis Chasma quadrangle, Venus.

Latitude	Longitude	Transect (km)	Wavelenth (m)	Orientation
–25.58	134.74	9.4	303	NE
–30.35	129.70	8.6	345	NE
–31.63	133.75	20.9	380	NE
–34.34	132.10	18.9	402	NE
–30.95	137.09	18.9	449	SE
–29.59	130.09	30.8	453	NE
–32.46	130.61	12.0	462	NE
–30.80	134.42	35.6	468	N
–27.57	136.65	21.7	494	NE
–32.15	130.93	27.2	495	NE
–35.38	133.62	32.1	526	NE
–30.71	130.64	45.8	572	NE
–30.78	129.99	58.2	588	NE
–36.21	132.48	44.3	607	NE
–28.12	136.09	85.9	641	NE
–35.83	132.13	48.0	657	NNE
–30.22	128.17	91.1	729	NE
–28.68	130.33	75.3	731	NE
–40.69	130.57	44.7	952	NE
		Average	540±157 (1σ)	
		excluding outlier	517±125 (1σ)	